Cooling, Collisions and non-Sticking of Polyatomic Molecules in a Cryogenic Buffer Gas Cell

A dissertation presented

by

Julia Hege Piskorski

to

The Department of Physics

in partial fulfillment of the requirements

for the degree of

Doctor of Philosophy

in the subject of

Physics

Harvard University

Cambridge, Massachusetts

June 2014

Thesis advisor

John M. Doyle

Author

Julia Hege Piskorski

Cooling, Collisions and non-Sticking of Polyatomic Molecules in a Cryogenic Buffer Gas Cell

Abstract

We cool and study trans-Stilbene, Nile Red and Benzonitrile in a cryogenic (7K) cell filled with low density helium buffer gas. No molecule-helium cluster formation is observed, indicating limited atom-molecule sticking in this system. We place an upper limit of 5% on the population of clustered He–trans-Stilbene, indicating a measured He-molecule collisional residence time of less than 1 μs. With several low energy torsional modes, trans-Stilbene is less rigid than any molecule previously buffer gas cooled into the Kelvin regime. We report cooling and gas phase visible spectroscopy of Nile Red, a much larger molecule. Our data suggest that buffer gas cooling will be feasible for a variety of small biological molecules. The same cell is also ideal for studying collisional relaxation cross sections. Measurements of Benzonitrile vibrational state decay results in determination of the vibrational relaxation cross sections of $\sigma_{22} = 8{\times}10^{-15}$ cm^2 and $\sigma_{21} = 6{\times}10^{-15}$ cm^2 for the 22 (v=1) and 21 (v=1) states. For the first time, we directly observe formation of cold molecular dimers in a cryogenic buffer gas cell and determine the dimer formation cross section to be $\sim 10^{-13}$ cm^2.

Contents

List of Figures

List of Tables

Citations to Previously Published Work

Portions of this thesis have appeared in the in the following papers:

"Cooling, spectroscopy and non-sticking of trans-Stilbene and Nile Red", Julia Piskorski, David Patterson, Sandra Eibenberger and John M. Doyle. Submitted for publication. (2014)

"Vibrational relaxation cross sections in cold Benzonitrile-helium collisions and the formation of Benzonitrile molecular dimers in a cryogenic buffer gas", Julia Piskorski, David Patterson and John M. Doyle. Submitted for publication. (2014)

Acknowledgments

I would like to thank my husband Andy, my parents and my family for their support throughout graduate school. You've given me strength and advice when I've asked for it. I thank Miles for bringing a smile to my face.

I thank my adviser John Doyle for his support, patience and guidance over the past seven years.

I thank past and present members of the Doyle group for their advice and help throughout graduate school. I learned a great deal of physics and engineering from working with Dave Patterson, Hsin-I Lu, Ivan Kozyryev, Boerge Hemmerling and Matt Wright. I thank Nick Hutzler, Elizabeth Petrik, Yat Au and Edem Tsikata for all their helpful conversations over the years. I also very grateful to Garrett Drayna, Boerge, Nick, Dave and Aakash Ravi for lifting heavy portions of the apparatus countless times.

I thank the other members of the incoming class of 2007 keeping graduate school fun. I thank the staff for all their help, especially Carol Davis, Jan Ragusa, Jim MacArthur, Stan Cotreau and Sheila Ferguson.

Lastly, I thank Brenda, Faeda, Gabby, Helena, Jennie, Lane, Maria, Noha and all of the staff at Miles's daycare for caring for him while I finished this project. It gave me piece of mind to know that he was in your hands.

To my family

Chapter 1

Introduction

Recent advances in producing cold and ultracold samples of molecules are motivated in part by the promise of new science in the areas of cold and ultracold chemistry [3, 4], dipolar quantum gases [5] and precision measurement [6, 7, 8]. Many experiments in these fields have shifted from working with atoms to working with molecules since molecules offer a richer internal structure for pursuing new physics. In particular, many molecules have significant electric dipole moments that can be fully polarized in the lab frame by laboratory accessible fields, allowing for the study of long range and anisotropic dipole-dipole interactions. Such interactions are essential for realizing certain quantum computation schemes [9] and for simulating increasingly complex Hamiltonians with dipolar molecular gases [10].

When cooled to temperatures of around 1 kelvin, a molecule's kinetic energy is comparable to the energy of its dipolar interaction with external electric fields. Collisions and chemical reactions may therefore be controlled in such systems by tuning external fields [11]. Some molecules offer energy levels that are uniquely sensitive

to fundamental quantities, allowing for sensitive probes of the electron's electronic dipole moment [6, 7] and the time dependence of fundamental constants [12]. Innovations in methods to cool diatomic molecules to lower temperatures have facilitated experiments in all of these areas [5, 8].

1.1 Cold polyatomic molecules

Most of the work with cold molecules focuses on polar diatomic molecules, yet samples of cold, polyatomic molecules are also of interest for spectroscopy [13, 14, 15], collisional studies [16, 17], chemical studies, chiral analysis [18, 19] and mixture analysis [20]. Spectroscopy of biological molecules in supersonic jets permits the characterization of properties of different conformers and may enhance the understanding of the connection between structure and function in biological systems [21, 22, 23]. Collision dynamics for cold molecules can be modified with long-range dipole-dipole interactions, and one can observe state-selective collisions [24, 16]. Also, many chemical reactions of neutral and radical molecules proceed with high reaction rates at the low temperatures [25] that are typical of conditions found in inter-stellar clouds and in the upper atmosphere [16].

Molecules that are important in biology and pharmacology exhibit a distinct handedness in interactions and reactions, yet distinguishing between different enantiomers still proves to be challenging. A newly developed technique, chiral analysis with microwave three-wave mixing, can sensitively measure the enantiomeric composition of a cold molecular sample [19, 26, 18].

With standard mixture analysis techniques, identifying and quantifying hundreds

of components in real world mixtures, such as human breath and blood, remain difficult for sensitive analysis techniques [27]. The simplification achieved in UV and microwave spectra of molecules at low temperatures readily lends itself to the identification of components in complex mixtures [20].

While several methods can generate samples of diatomic molecules at low temperatures [28, 29, 11, 30], only two methods, supersonic jet expansion combined with Stark deceleration [31, 32] and buffer gas cooling [33, 34, 17], have produced cold, slow polyatomic molecules in the lab frame. While cold, molecular sources of radicals have been produced with both methods, buffer gas based beams have higher fluxes than supersonic expansions [35]. The ability to produce continuous buffer gas beams allows an increase in molecular flux of up to three orders of magnitude for stable molecules with significant vapor pressures at room temperature, including ammonia [35].

Although the cooling of a supersonic expansion alone is sufficient for spectroscopy and chiral analysis of molecules, sources of cold, slow large molecules are particularly beneficial for collisional studies, chemical studies and mixture analysis. To date, only one method, Sisyphus cooling in electrical traps, has been demonstrated to cool polyatomic molecules to even lower temperatures [36]. Extension of these cooling techniques to larger, perhaps biological, molecules could be beneficial for improved analysis of biological samples and fundamental studies of collisions and reactions.

1.2 Buffer gas cooling

Buffer gas cooling is a general method for cooling atoms and molecules to low temperatures and has been demonstrated for numerous atoms [37, 38], as well as diatomic molecules [39, 40] and more recently, polyatomic molecules [34]. Prior to this work, molecules comprised of up to 23 atoms had been successfully buffer gas cooled [41]. In this work, we explore cooling of larger and structurally more complex molecules with significantly softer modes using this technique.

Buffer gas cooling relies on elastic collisions between cold buffer gas atoms and initially hot molecules to cool both internal and external degrees of freedom. Although the technique efficiently cools translational and rotational degrees of freedom, quenching of vibrational states proceeds more slowly as a result of a mismatch between a collision timescale and vibrational period [42]. Consequently, the translational and rotational temperatures of a molecular gas thermalize rapidly to the temperature of the buffer gas, yet the vibrational state population distribution may remain out of equilibrium for some period of time. For example, a small population of CaH molecules remained in the first vibrationally excited state after colliding with 0.5 K He-3 for nearly a second, and the vibrational relaxation rate coefficient for the v=1 state of CaH was measured to be less than 10^{-16} cm^3s^{-1} [43]. For the vibrationally excited states of some molecules, collisional quenching proceeds slowly enough to observe directly in the cell, as is the case in the experiment discussed in this thesis. We describe measurements of collision quenching cross sections for two vibrational states of Benzonitrile in Chapter 4.

Since buffer gas cooling requires a significant vapor pressure of cold, inert gas-

phase atoms, the method is limited to temperatures of ∼15 K for neon, ∼1 K for helium-4 and ∼200 mK for helium-3. To date, most of the work with polyatomic molecules has used ∼5 K helium-4 buffer gas, but with a few technical modifications, molecules should be able to be easily cooled to ∼1 K with helium-4. Any additional cooling below these temperatures requires a separation of the species from the buffer gas, which is typically achieved by confining a species with external fields [44, 45, 46].

Since buffer gas cooling requires elastic collisions with cold, buffer gas atoms, we expect it to fail when the buffer gas sticks to a molecule, and one would expect to end up with cold molecules embedded in a small cluster or nano-droplet. Understanding the process of how the first buffer gas atom sticks to a molecule is crucial (and of significant intellectual interest in itself), but we have no understanding of which molecular properties would drive this sticking process. Stable cluster formation requires three bodies to satisfy conservation of energy and momentum and may proceed either directly via three body recombination or through the Lindemann mechanism [47]. In the latter case, a molecule and a helium atom form a short-lived collision complex. Since typical in-cell buffer gas densities are low enough that direct three body recombination rates (ie. 'instantaneous three-body collisions') are low, we instead expect this process to proceed at a significant rate when an atom and a molecule form a collision complex whose lifetime or residence time is long compared to the typical time between collisions in the buffer gas [34, 48].

One approach to understanding the mechanism of atom-molecule cluster formation is to seek out and study molecules that are likely to form longer-lived collision complexes. The details of the relationship between molecular properties and the resi-

dence times remains poorly understood, but collision complexes containing molecules that have many internal states with energies less than a cluster binding energy are expected to have longer residence times [49]. Molecules with low energy vibrational modes and larger molecules with many internal degrees of freedom are therefore more likely to form long-lived collision complexes. A detailed discussion of theoretical predictions about the residence time can be found in Section 2 of Chapter 3.

In this work, we explore some of these questions by studying the cooling of a molecule with many low energy torsional modes, trans-Stilbene and a molecule comprised of 42 atoms, Nile Red. We observe no signs of helium-molecule cluster formation for either molecule and place a limit on the lifetime of the He–trans-Stilbene complex.

1.3 Van der Waals clusters

Although the onset of cluster formation in a buffer gas could limit the utility of buffer gas cooling, van der Waals clusters themselves are a rich field of study [50]. In van der Waals clusters, intermolecular forces weakly bind atoms and molecules together, and as a result, such dimers and larger clusters can provide insight into phase transitions at the molecular level. Characterization of clusters can aid in understanding the connection between intermolecular forces and bulk matter [51]. For example, many isomers of water clusters resemble structures that are observed in water for brief timescales, and the study of various sized water clusters enhances an understanding n-body terms in the intermolecular potential [52]. Water and ice are fundamental to the natural world, yet their properties cannot be accurately modeled

from molecular dynamics alone [53].

Although dissociation energies for dimers are on the order of a hundred times smaller than those of molecular bonds, small clusters with less than ten constituents can still have well defined rotational and vibrational states [54]. Studies of van der Waals clusters focus on characterizing the low frequency intermolecular vibrational modes, binding energies and conformal isomers of van der Waals clusters [55]. Van der Waals clusters have been studied and observed in both equilibrium gas phase conditions [54, 56] and out-of-equilibrium supersonic beams[50, 14].

1.3.1 Spectroscopy in Supersonic Jet Expansions

Supersonic beams provide an effective tool for studying the spectroscopy of carrier gas–molecule clusters. The primary spectroscopic signature of cluster formation in a supersonic beam is the appearance of equally spaced lines to the red or blue of the strongest molecular lines as the expansion backing pressure is increased [57, 58]. Mass spectrometry experiments confirm that these lines typically correspond to carrier gas–molecule complexes [59, 60]. Typical spectral shifts for helium-molecule clusters range from 1 to 8 cm^{-1} per helium depending on the molecule [14, 13], and helium-molecule clusters have some of the smallest spectral shifts observed for any complexes [57]. Both molecular dimers and bi-molecule complexes have also been studied in supersonic beams.

1.3.2 Formation

While the characteristics of clusters in supersonic beams are well known, their formation is not well understood. Most clusters form in the high density and intermediate temperatures of the initial expansion and then cool [61]. Formation of van der Waals clusters in helium nanodroplets suggest that the dimers formed in supersonic jets do not form the lowest energy conformers, consistent with formation at an intermediate temperature [62]. While the potential energy surface for some atom-molecule pairs have been calculated based on the experimental data, these calculations are limited to diatomic and triatomic species [63].

Ultimately, the formation of complexes in supersonic expansions limits the lowest temperatures achievable with the technique [64]. Both larger binding energies and larger cross sections are known to lead to more rapid cluster formation in supersonic beams [61]. Since typical helium-molecule binding energies and cross sections are smaller than other those of other atom-molecule combinations, the choice of helium as a carrier gas can reduce cluster formation and permit cooling to lower temperatures [64]. In this thesis, we explore the existence of a similar limit for buffer gas cooling and study He-molecule collisions at energies well below their binding energy, in which the pair would form a dimer (or a larger cluster) under equilibrium conditions.

Chapter 2

Experimental Overview

Molecules from an oven source flow through an aperture into a cold (5K) cell filled with helium buffer gas. After approximately 100 collisions with helium atoms, molecules that reach the central region of the cell are translationally and internally cold. Molecules are detected via laser induced fluorescence (LIF) in two regions of the cell. With this system, vibrational spectroscopy, collisions, clustering and dimer formation is studied.

2.1 Molecular Source

The work described in this thesis focuses on molecules that either have a significant vapor pressure at room temperature or have a significant vapor pressure when gently heated. Since many larger polyatomic molecules have low vapor pressures and are thermally labile, this method for transferring a species into the gas phase limits the classes of molecules available for study. Many biological molecules are not generally

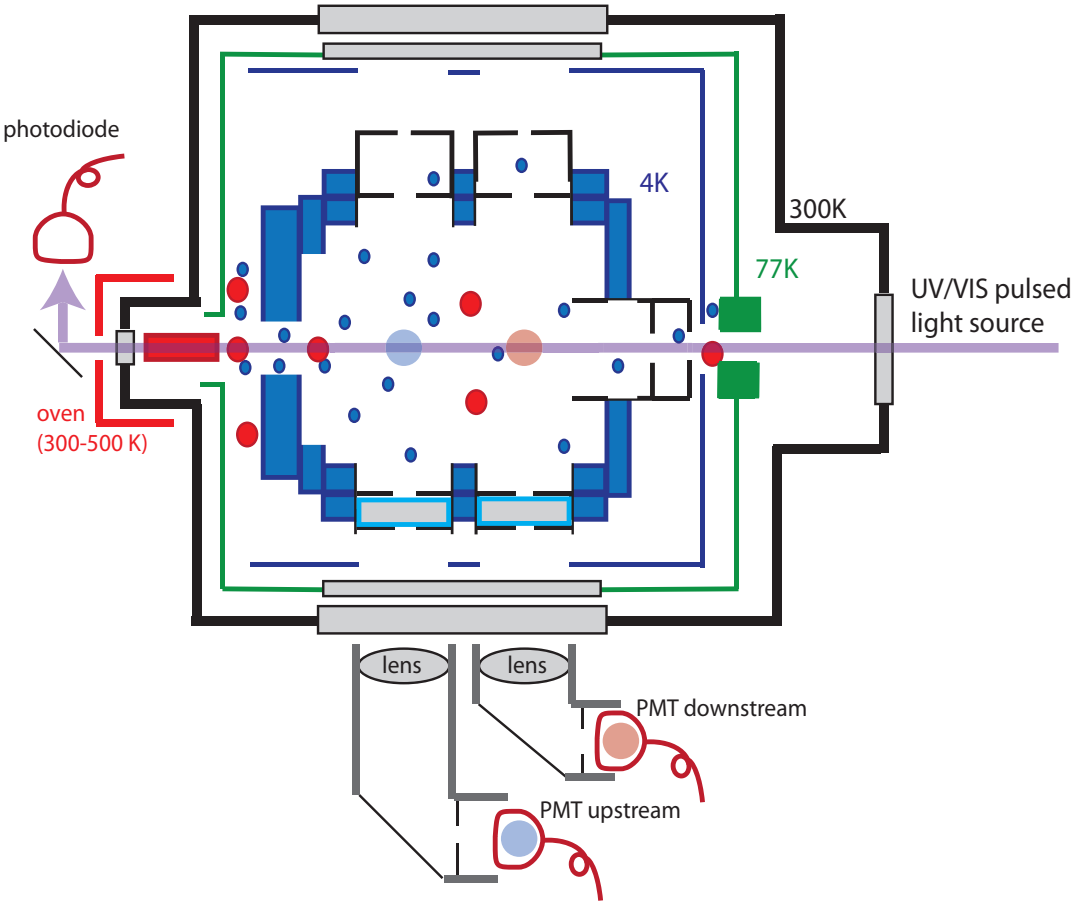

Figure 2.1: Warm molecules cool after colliding with cold helium buffer gas. Only cold molecules reach the cell interior where they are detected via LIF.

suited to oven sources since they decompose upon heating. Alternative methods for vaporizing large molecules will be discussed in Chapter 5 Section 1.3.

Molecules flow down an 8 inch long and 0.375 inch diameter heated copper tube that protrudes through the radiation shields directly into the coldest region of the apparatus, with the end sitting 0.5 inch away from an aperture in the front face of a cold (6-7.5 K) cell, as shown in figure 2.1. To reduce black body heat loads while still maintaining a high conductance, the tube narrows to a 0.25 inch diameter for the final inch. Most of the copper tube is wrapped in several layers of aluminized

mylar. Resistive cartridge heaters allow the tube's temperature to vary from 300-500 K. Figure 2.2 provides an overview of the entire molecule injection manifold.

2.1.1 Room temperature injection

For molecules with sufficient vapor pressure at room temperature, molecular flow may be controlled by adjusting the pressure of the molecular vapor in the gas manifold before the long copper tube. Liquid molecular samples may be injected into the sample region through a thin piece of teflon with a 25 gauge syringe. Solid molecules may be loaded into the reservoir by opening a KF flange.

A needle valve and a higher-conductance bellows valve allow for fine control of the molecular backing pressure in the gas manifold connected to the sample reservoir. Molecular pressures in the manifold are measured by a Grandville Phillips 275 mini convectron gauge. The long, narrow copper tube sets the conductance of the molecule injection line, which is estimated to be 0.15 liters/sec. Molecular flow f may be calculated from the pressure P and conductance C by the following [65]:

$$f = PC.$$

Typical molecular flow rates for Benzonitrile are estimated to be $\sim$3 sccm $\pm$1 sccm.

2.1.2 Oven source

Molecules without significant vapor pressure at room temperature require heating to provide enough molecular flow for detection. Powdered samples are placed into the oven manifold by breaking and replacing a conflat seal on the oven manifold.

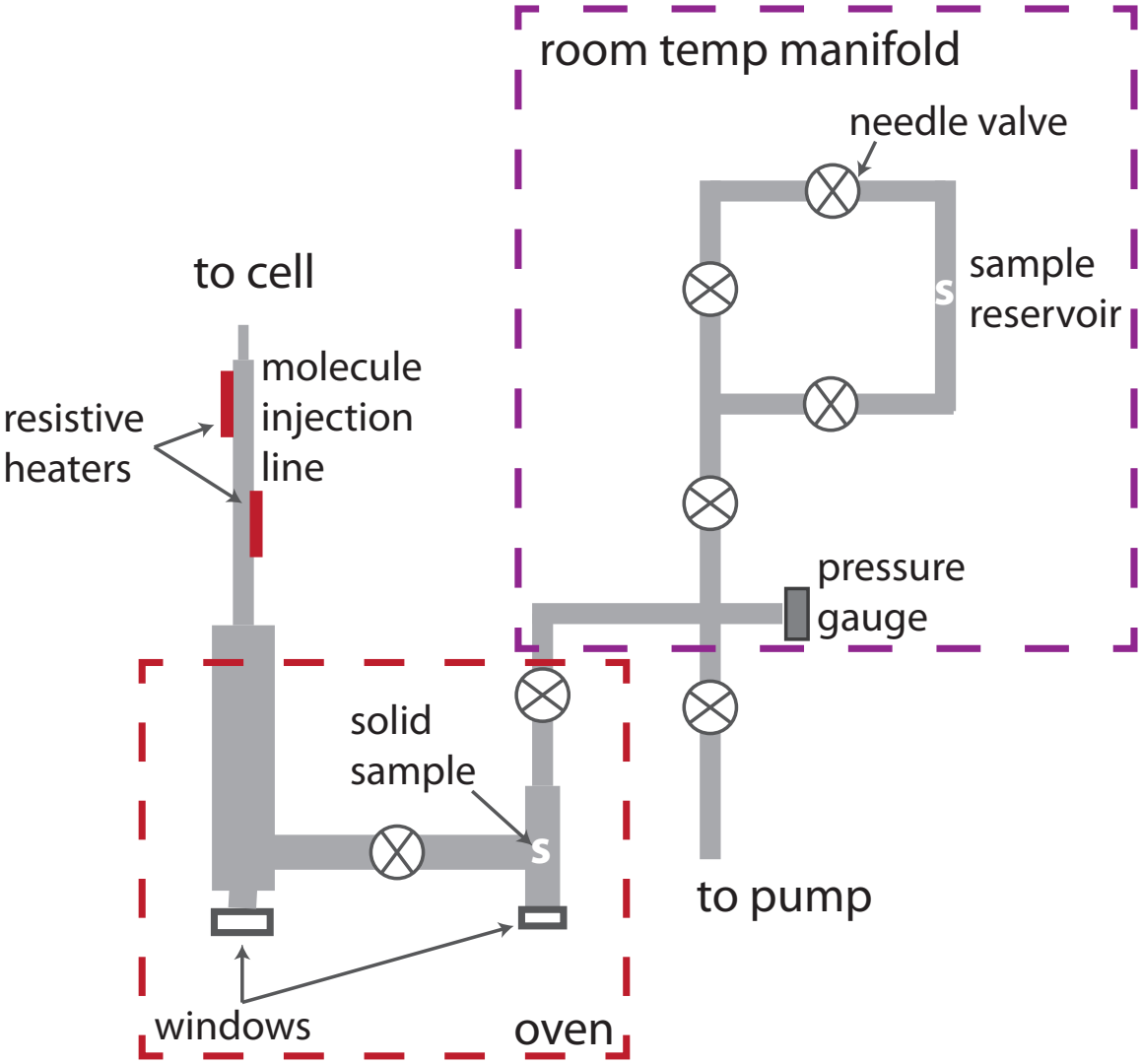

Figure 2.2: Molecule injection manifold for oven or room temperature operation. Solid and liquid samples may be loaded into a room temperature manifold, and valves control the pressure in the oven manifold and flow of molecules into the cell. For oven operation, samples are loaded directly into the oven manifold, and the oven temperature directly controls the flow of molecules into the cell.

Since molecules readily vaporize when heated, care must be taken to ensure that the exterior of the oven manifold is kept free of residual sample and cleaned after sealing as a safety precaution.

The entire oven manifold fits into a modified commercial lab oven QL model 10, and additional resistive heaters along the copper line and around a few cold spots permit the entire molecule injection line to be heated relatively uniformly, within a 10 K range, to temperatures of 500 K. Two types of components in the manifold, CF windows and KF o-rings, set a maximum temperature of 500 K for the oven manifold; however, the operational performance of the system as a whole indicates that this temperature also corresponds to the maximum black body heat load that the cryostat can reasonably handle.

Valves at either end of the oven permit it to be sealed from the main copper line and a room temperature molecule injection manifold. Without a pressure gauge inside the oven, precise molecule flow rates are unknown. Based on the heat loads on the cell from molecule condensation, we estimate that typical molecule flow rates (from the oven line) are 4 sccm $\pm$ 2 sccm. The temperature of the oven solely controls molecular flow rates into the cell, and the temperature was tuned to provide ample signal in the cell.

2.1.3 Requirements for molecules of study

We select molecules compatible with the oven requirements described above and also focus on molecules with well characterized UV and visible spectroscopy where possible. Since this experiment requires frequent breaking of vacuum and cleaning,

we chose to work with molecules that posed little health risks. Many biological molecules can have significant health effects if ingested, inhaled or absorbed through the skin, even in quantities of tens of micrograms. Since we did not find a biological molecule that met our oven, spectroscopy, molecular size and health requirements, we compromised by choosing to work with Nile Red, which meets the oven, size and to the best of our knowledge, health concern requirements. After completing this experimental work, we found a thin layer of Nile Red coating the interior of the entire 300 K vacuum chamber, even in regions with no direct line of sight to the molecule injection line.

2.2 Cryogenic cell

The molecules from the oven flow through an aperture into a cold (5 K) cell filled with helium buffer gas. The cell and oven geometry are similar to that described in reference [41]. A hot 0.25 inch copper oven aperture and the cryogenic cell are separated by about 0.5 inches, to reduce parasitic heat loads on the cell. Molecules flowing from the oven toward the cell begin to collide with cold helium buffer gas just outside the cell. Simulations estimate that about 20% of molecules flowing from the oven reach the cell interior [41].

2.2.1 Physical geometry

Molecules flow into a 0.5 inch hole in the side of a copper and aluminum cryogenic cell, shown in figure 2.4. As the largest hole in the cell, the aperture in the cell sets the overall in-cell helium density. The size was chosen to keep the density low enough

Figure 2.3: Nile Red residue on a chem wipe swab from the near the top of the 300K vacuum chamber in a region with no direct lines of sight to the molecule injection line. A thin coating of Nile Red on the entire 300 K vacuum chamber indicates that even molecules with very low vapor pressures can reach anywhere within the vacuum system.

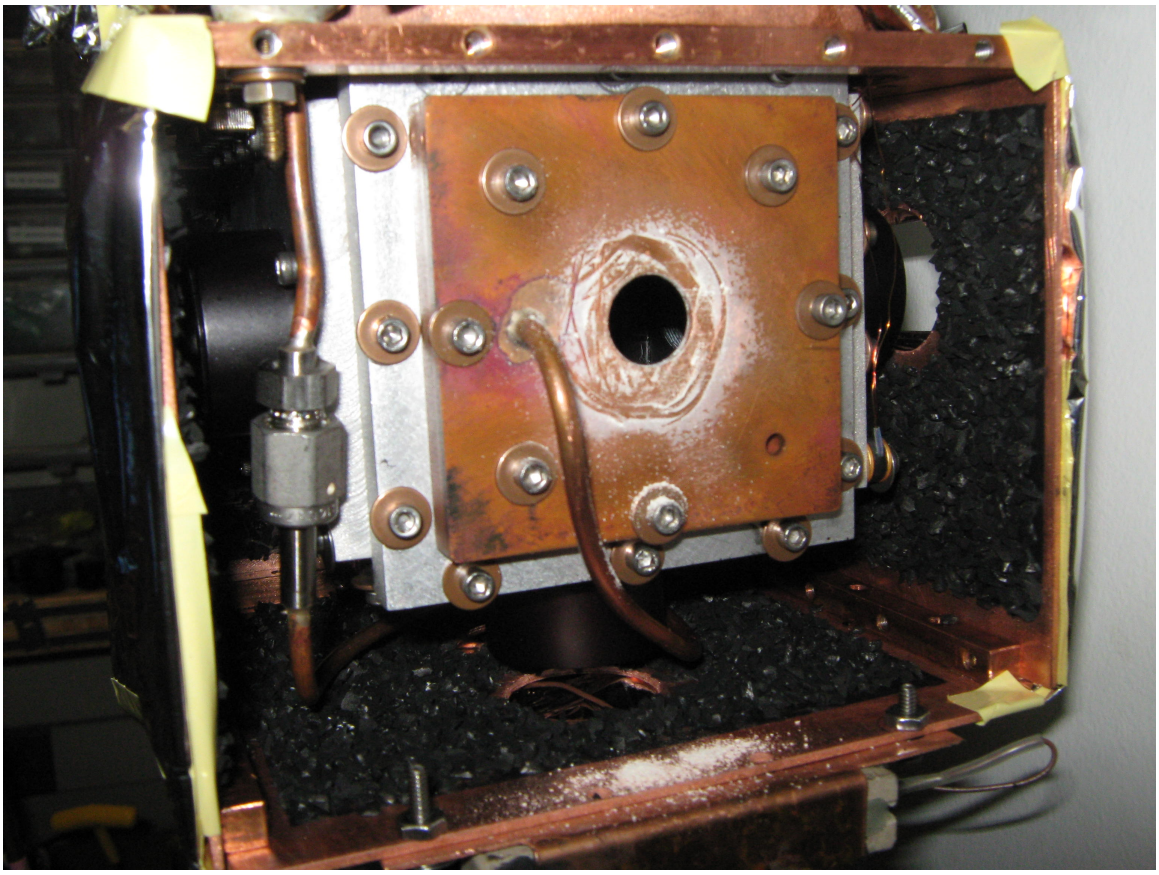

Figure 2.4: Molecules flow through an aperture in the side of a cold copper and aluminum cell. Here one can see a thin layer of melatonin deposited on the cell exterior. Coconut charcoal sorbs surrounding the cell pump helium, and the cell nearly fills the entire available experimental space.

for molecules to flow into the cell yet high enough for molecules thermalize to the temperature of the helium long before reaching the cell walls. Typical in cell helium densities range from 1–5 $\times$ 10^{14} cm^{-3} for helium flow rates of 2–9 sccm. A detailed discussion of the collision environment in the cell follows in the Section 2.2.

With dimensions of 2.5 by 2.5 by 3.5 inches, the cubic cell nearly fills the entire cold region of the apparatus and limits the available space to fit additional coconut charcoal sorb. The experimental cell is nearly identical to the cell described in ref

[41]. A second, 0.25 inch aperture, opposite the molecule input aperture, allows detection light to pass through the cell without transmitting through and consequently, scattering off a window. Two windows in the cell allow molecules to be detected via laser induced fluorescence, as shown in figure 2.1. Molecules undergo collisions with helium and potentially other molecules while traveling the 1.25 inches between the 'upstream' and 'downstream' detection regions, as is discussed in more detail in section 2.2.2.

Since this experiment requires macroscopic quantities of non-reactive molecules with low vapor pressures, we can observe molecule deposition in the cell interior upon opening the chamber and confirm our assumptions about the relative quantities of molecules reaching different regions of the cell. However, the downside of this feature is that we observe significant molecular deposition on the detection windows after a day of running. Cleaning the windows requires warming up the chamber to room temperature and breaking vacuum. Figure 2.5 shows the upstream and downstream windows after one day of running with Nile Red. The 'upstream' window has a thicker coating of molecules on it than the 'downstream' window. To facilitate easy cleaning of the windows between runs with acetone, these windows may be accessed through the side of the cryostat without requiring a full disassembly. All cell windows and apertures are mounted in lens tubes to allow for easy removal and geometry modifications, as shown in figure 2.6.

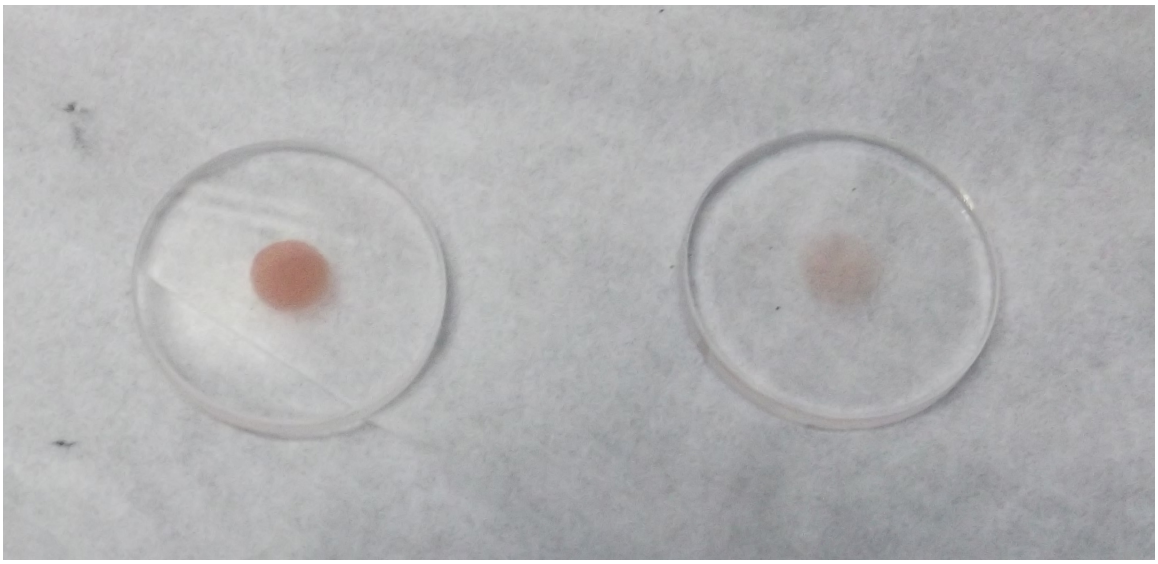

Figure 2.5: Picture of molecular deposition after a one day run with Nile Red. A thicker layer of molecules are deposited on the upstream cell window (shown on left).

Figure 2.6: Cell windows and baffles are mounted into lens tubes for easy cleaning and modification. Pink residue is a thin layer of Nile Red.

2.2.2 Collision environment in the cell

Large molecules require about 50–100 collisions with cold helium atoms to cool rotationally and translationally to close to the buffer gas temperature [41], and FTMW spectroscopy in a similar cell confirmed that molecules thermalize to the temperature of the buffer gas, approximately 7 K [41]. Due to limitations in our optical detection in this experiment, we were not able to directly determine the temperature of the molecules to better than an upper bound of 40 K, but we expect them to be at a temperature of approximately 7 K based on the FTMW data and simulations of the buffer gas temperature described in Chapter 3.

Once inside the cell, molecules typically undergo an additional 100 collisions before reaching the cell walls, a process that takes a few milliseconds. Typical helium flow rates of 2–9 sccm correspond to estimated in-cell helium atom densities of 1–5$\times10^{14}$ cm^{-3} $\pm$ 1$\times10^{14}$ cm^{-3}. At a typical density of 2$\times10^{14}$ cm^{-3}, a typical mean time between helium collisions is 50 μs. In contrast to supersonic jet expansions, molecules in the buffer gas undergo collisions only with 5 K helium atoms at low densities ($\approx$ 10^{14} cm^{-3}) throughout the cooling process and continue to collide steadily with the buffer gas while traversing the cold cell. As a result, any cluster formation occurs under cold, low density conditions.

Between the two in-cell detection regions, molecules collide with helium atoms, and potentially other molecules. While helium-molecule and molecule-molecule elastic cross sections are not known in detail for Benzonitrile, trans-Stilbene and Nile Red, we can conservatively estimate that they are similar to or greater than rotational relaxation cross sections measured for other large molecules [41]. Based on the helium

atom and molecule in-cell densities and our estimated elastic cross sections between 3–5$\times 10^{-14}$ cm^2, we calculate that molecules collide about 200 times with helium atoms as they travel between the two detection areas.

Based on the heat loads on the cell from molecule condensation, we estimate that typical molecule flow rates (from the oven line) are 4 sccm $\pm$ 2 sccm, and a corresponding in-cell molecular density of 2×10^{12} cm^{-3} $\pm$ 1×10^{12}. At these densities, the estimated time between molecule-molecule collisions is approximately 10 ms, so only about 5% of the in-cell molecules collide with other molecules before reaching the cell walls.

At first glance, a low density helium cell seems like a poor choice for studying clustering of large molecules with helium buffer gas since cluster formation proceeds more rapidly at higher densities. Molecules only collide with cold helium throughout the cooling process, and this molecule injection method allows for control over conditions of any molecule-helium cluster formation. Alternative system geometries have oven sources directly connected to a higher density cell. In contrast to a low density cell with a close by, but unconnected, molecule injection line, a cell with a connected molecule injection line relies on helium carrier gas to sweep molecules into the cell interior [33, 34]. Molecules and helium collide at a range of temperatures, making it nearly impossible to understand conditions of any cluster formation. A flow tube method for introducing molecules also places larger heat loads on the cell, limiting the maximum oven temperature and consequently, which molecules may be studied.

2.3 Optical Detection

After reaching the cell interior, molecules are detected by laser induced fluorescence. Light from a pulsed Optical Parametric Oscillator shines through the length of the cell and down the molecule injection line. Since the OPO has unusual spacial modes, careful shaping with lenses and irises ensures that it does not clip on the molecule injection line, and figure 2.7 shows the shaping optics and optical path of the OPO light through the apparatus. Fluorescence is collected in two regions of the cell: 'upstream' and 'downstream', located 1.125 inches and 2.375 inches respectively from the cell aperture.

2.3.1 OPO

The light source for LIF is a pulsed Optical Parametric Oscillator (OPO) by Spectra Physics. With a linewidth of 7 cm^{-1}, the OPO can easily resolve vibrational lines but not rotational lines. Linewidths in all observed spectra are limited by the OPO linewidth. Although recent advances in OPO technology have given rise to continuous OPOs with narrower linewidths, we did not have such a light source available to us. Despite the large linewidth, the wide tunability of the OPO (260-350 nm and 410-709 nm) makes it as easy as a couple of keystrokes on a computer and a few teaks of steering mirrors to switch wavelengths to work with a new molecular species. A Photon Control spectrometer SPM-002 independently monitors the wavelength of the OPO.

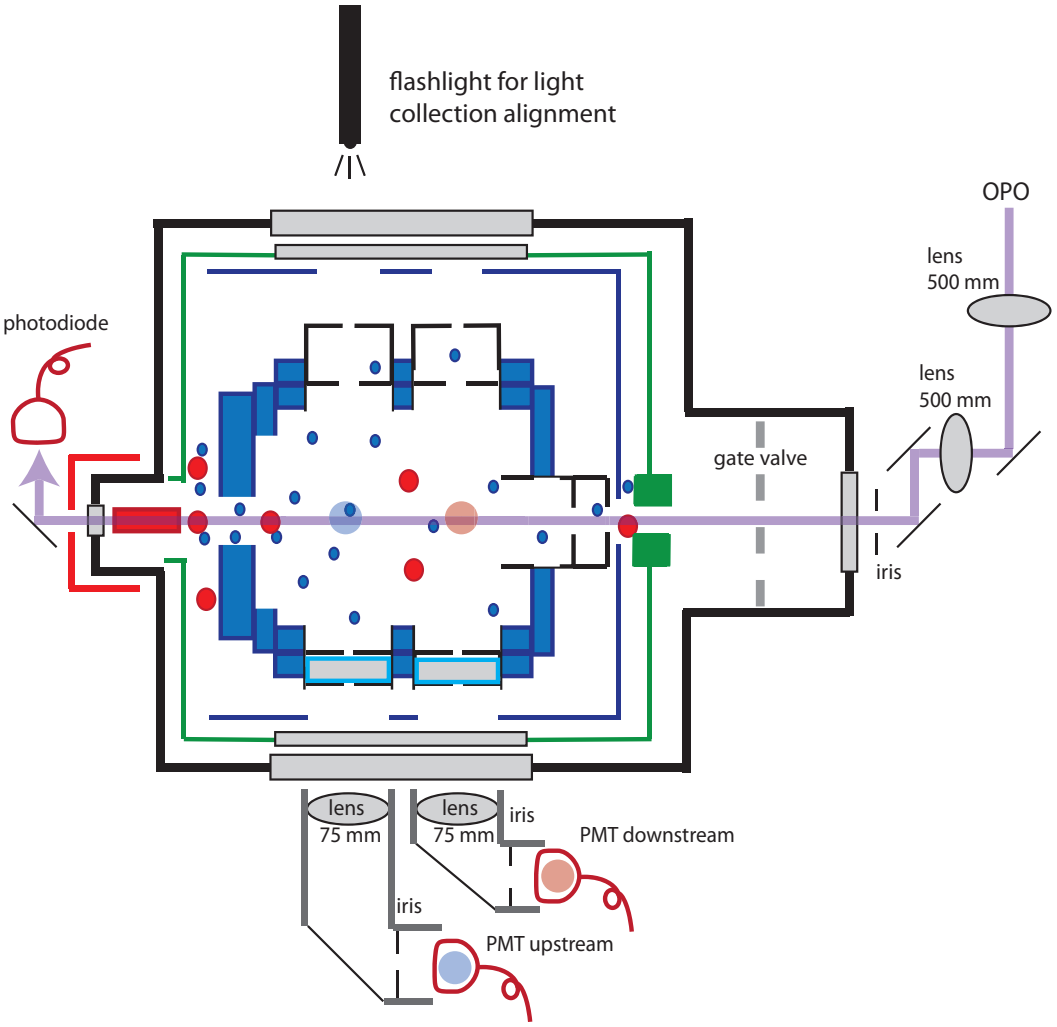

Figure 2.7: An overview of the OPO path through the cell and light collection optics.

2.3.2 Optical path through the cell

As the OPO light traverses the chamber, it travels through small apertures in the radiation shields, and the only windows that the light passes through are two borosilicate windows on the exterior vacuum chamber. While holes in radiation shield contribute significantly to higher heat loads on the cell, an absence of interior windows along the OPO path reduces scatter into the light collection optics and removes surfaces on which molecules may be deposited. Significant molecule deposition on a cell window could also reduce the power of the OPO light transmitted through the apparatus and shorten the effective experimental time.

Preventing a buildup of molecules on windows along the OPO path becomes critical for molecules from heated oven sources because removal of deposited molecules requires venting the chamber and cleaning of surfaces with solvents. Molecules from room temperature sources will simply evaporate as the chamber warms up under vacuum. A gate valve prevents significant molecule deposition on the room temperature window through which the OPO enters the vacuum chamber, and this gate valve allows for removal and cleaning of the window while the apparatus remains cold and under vacuum.

Light from the OPO passes through the molecule injection line and out a second, heated vacuum window in the oven. We have not observed any significant molecule deposition on the window in the oven. Several optics shape the light from the OPO to prevent it from clipping on parts of the cell interior and scattering into the light collection optics.

2.3.3 Light collection for fluorescence

Laser induced fluorescence is collected through two 0.25 inch diameter windows in the cell. Several baffles in the cell interior help to reduce scattered light from reaching the PMT. Fluorescence light is collected through two windows in the cell that are separated by 1.25 inches. Outside the chamber, a 75 mm lens collects a little less than 1 percent of the light emitted by fluorescing molecules and focuses the light onto a Hamamatsu R9880U-01 photomultiplier tube, as shown in figure 2.7. An iris in front of the PMT helps to reduce scattered light from reaching the PMT.

Scatter from the OPO is a dominant source of background noise in the raw data and is reduced effectively through careful alignment and shaping of the OPO path through the cell and use of long pass filters for Nile Red. The response curve of the PMT is such that the it is far more sensitive to the fluorescence from Benzonitrile and trans-Stilbene rather than UV light from the OPO, and no filters were required to achieve good signal to noise for these molecules. An excellent rough alignment for the light collection optics is achieved by shining a flashlight through a pin hole on the opposite side of the cell. A picture of the entire experiment is shown in figure 2.8.

2.4 Cooling to low temperatures

The entire apparatus is built upon a modified Infrared Laboratories HDL-5 dewar that consists of a 0.8 liter nitrogen bath and a 1.2 liter helium bath. The IR labs insert is shown in figure 2.9. Each bath cools an associated radiation shield, and the cell maintains a low temperature (7 K) for up to 3.5 hours with typical room

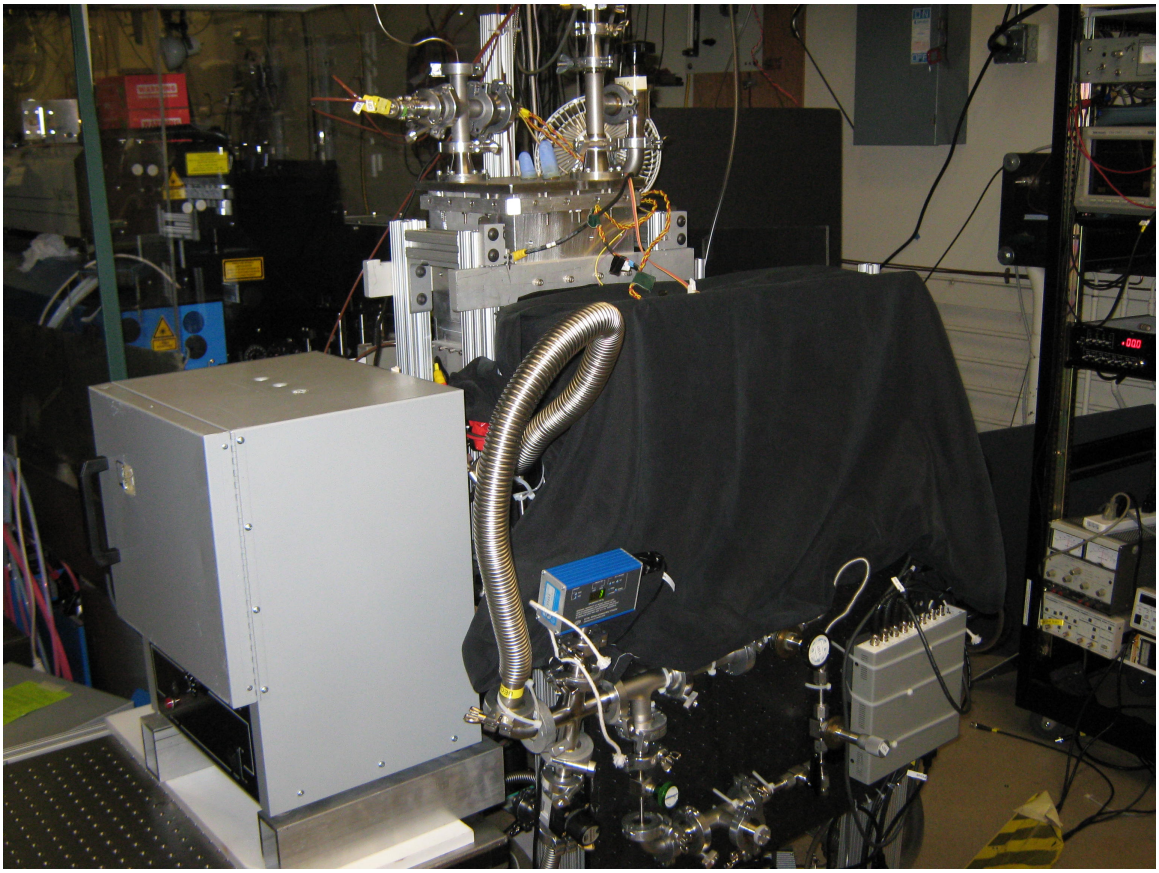

Figure 2.8: A picture of the entire experimental setup. From left to right, we see an oven used for heating the oven manifold, a vacuum chamber with an IR labs insert, a light collection system (covered in black cloth). Below, we see a gas manifold for room temperature molecular samples. The bulk of the experiment fits on a single table.

temperature molecule flows. With the molecule injection line heated to ∼500 K, an increased heat load shortens the typical chamber cold time to 1.5 hours. This additional heat load causes the temperature of the coconut charcoal sorbs to rise to 7 K, a temperature at which they have a noticeably reduced helium pumping speed and capacity. Studying molecules that require oven temperatures above 500 K would not be feasible in the current system; however, working with higher oven temperatures should be reasonable in a pulse tube based apparatus that has up to 1.5 Watts of cooling power and room for additional charcoal sorb.

2.4.1 Heat loads

Based on the hold times for the chamber, the total average heat load on the helium bath is estimated to be 0.3 watts for room temperature operation and 0.7 watts for oven temperatures of 500 K. Measuring the difference in cell temperature with and without molecular flow, we estimate a heat load of 0.2 W ± 0.05 W from the deposition of hot molecules into the cell. Both the conductive heat load of the helium and molecules as well as black body heat loads from the molecule injection line and a 0.5 inch diameter hole in 77 K shield contribute to heat loads.

2.4.2 Reducing black body heat loads

The molecule injection line and an second aperture in the 77 K radiation shields create significant black body heat loads on the helium bath. At 500 K, the estimated black body heat load on the cell from the molecule injection line rises to 0.12 watts. To mitigate this heat load, two cold lens tubes extend around each aperture to reduce

Figure 2.9: The experimental cell is mounted to the bottom of an IR labs dewar and cooled with liquid nitrogen and liquid helium. The cell nearly fills the entire 4 Kelvin region.

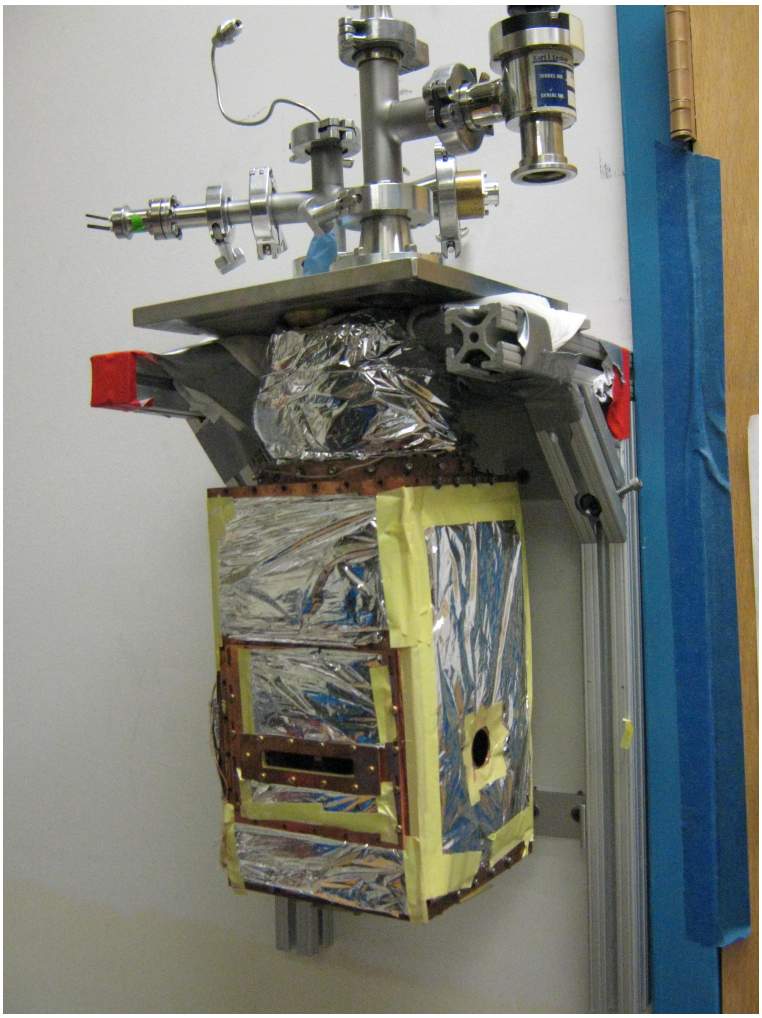

Figure 2.10: IR labs dewar with nitrogen radiation shield surrounding the cell. This entire assembly is inserted into a 300 K vacuum chamber during normal operation.

the radiation reaching the coldest regions of the chamber. The lens tubes reduce the black body heat load by roughly a factor of 4 over a simple circular aperture in an shield. This method for reducing heat loads should be applicable in many cryogenic systems.

Chapter 3

Cooling, spectroscopy and non-sticking of trans-Stilbene and Nile Red

We create and study trans-Stilbene and Nile Red in a cryogenic (5K) cell with a low density helium buffer gas. No molecule-helium cluster formation is observed, indicating limited atom-molecule sticking in this system. We place an upper limit of 5% on the population of clustered He-trans-Stilbene, indicating a measured He-molecule collisional residence time of less than 1 μs. With its very low energy torsional modes, trans-Stilbene is less rigid than any molecule previously buffer gas cooled into the Kelvin regime. We also report cooling and gas phase visible spectroscopy of Nile Red, a much larger molecule. Our data suggest that buffer gas cooling will be feasible for a variety of small biological molecules.

3.1 Clusters in equilibrium

In equilibrium, the distribution of molecular energies includes a small fraction of molecules with enough energy to initiate processes inaccessible to the mean thermal energy. Consequently, a fraction of molecules may be found in dissociated states, and the relative number of free molecules will depend upon the temperature, binding energy and densities in the system [66, 56]. A significant population of free molecules will be found even at temperatures well below the binding energy of a cluster.

Cluster formation requires three bodies in order to conserve energy and momentum, and the following reaction describes the equilibrium formation and destruction of helium-molecule dimers:

$$Mol + He + He \rightleftharpoons (Mol - He) + He.$$

For a system in equilibrium, the equation representing this chemical reaction can be rewritten as

$$Mol + He - (Mol - He) = 0$$

or, more generally,

$$\sum_i v_i Ai = 0$$

where v_i and A_i are the reaction coefficients and chemical species, respectively.

In equilibrium, the change in the Gibbs free energy of the system is zero, and as a result, any change in the number of a chemical species dN will depend on the corresponding coefficient v_i and the chemical potential μ_i of the species involved [67]

$$\sum_i v_i \mu_i = 0.$$

This implies that a change in the concentration of one reaction in equilibrium will cause a corresponding change in the concentration of other species.

The law of mass action describes the relative concentrations of the molecular products in terms of an equilibrium constant κ that depends on the temperature

$$[Mol][He][Mol-He]^{-1} = \kappa[67].$$

For an ideal gas, κ depends on the temperature T and is defined as

$$\kappa(T) \equiv \prod_i n_{Qi}^{vi} exp[\frac{-v_i BE}{k_b T}]$$

where BE is the cluster binding energy and n_{Qi} is the quantum concentration for each species [67]. The quantum concentration describes a density with one atom of mass M per cubic volume of a de Broglie wavelength

$$n_Q = (\frac{Mk_bT}{2\pi\hbar^2})^{\frac{3}{2}}.$$

In the case of molecule-Helium dimers, the reaction obeys the following

$$\frac{[Mol-He]}{[Mol]} = \frac{[He]}{n_{QHe}} exp[\frac{-BE}{k_b T}].$$

The fraction of unclustered molecules at equilibrium is then given by

$$\frac{[Mol]}{[Mol-He]+[Mol]} = \frac{1}{1+\frac{[Mol-He]}{[Mol]}}.$$

Although helium-molecule binding energies are unknown for the molecules studied, helium-molecule binding energies for many substituted benzene rings tend to be roughly 100 cm^{-1} [68]. Assuming this binding energy and an in-cell helium density of 4×10^{14} cm^{-3}, figure 3.1 shows the expected fraction of helium-molecule dimers

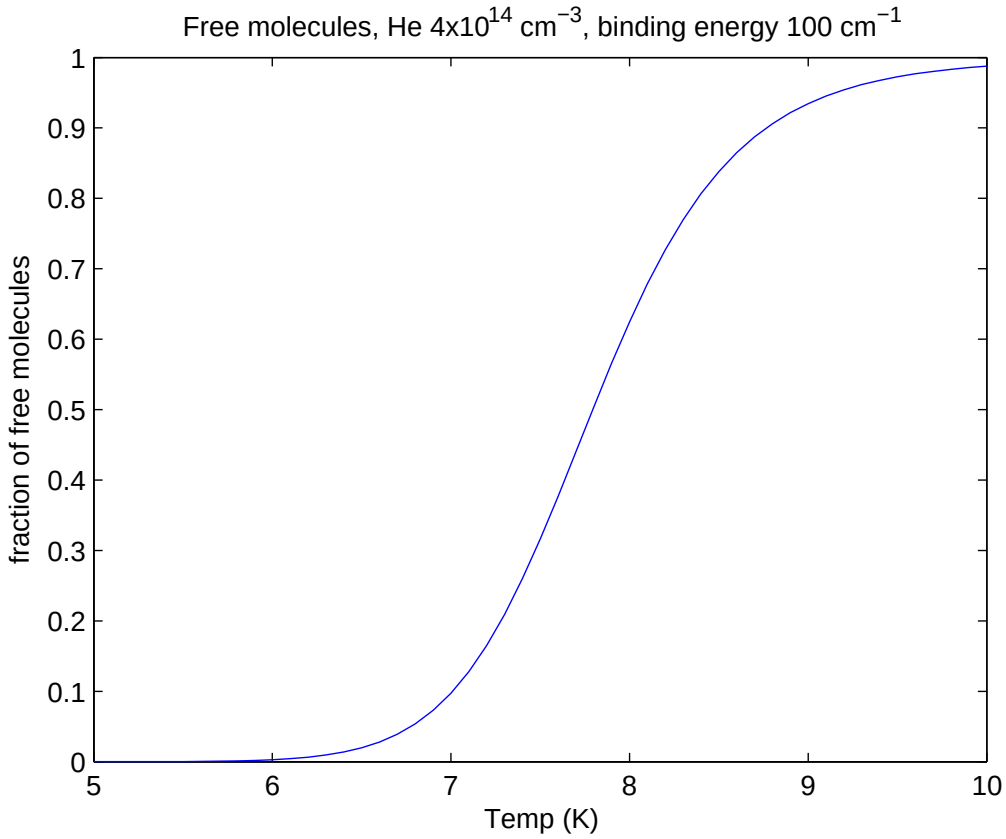

Figure 3.1: Fraction of free molecules in equilibrium as a function of temperature for a binding energy of 100 cm^{-1} and helium density of 4×10^{14} cm^{-3}. At a typical cell temperature of 7 K, the majority of molecules are clustered in equilibrium.

present under equilibrium conditions. At a temperature of 7 Kelvin, helium-molecule dimers are energetically preferred over free molecules, and thus, we expect that most molecules would be clustered with helium in equilibrium conditions.

Depending on the heat load from the oven, cell temperatures range from 6–7.5 K for the molecules studied. Table 3.3 summarizes the typical operation conditions of the cell for each molecule. The cell operates at temperatures at which cluster formation would be preferred in equilibrium for Benzonitrile and trans-Stilbene. The higher heat loads from the oven due to the higher temperatures necessary for Nile

Table 3.1: Calculated helium-molecule binding energies for several molecules.

molecule	binding energy cm^{-1}	reference
Benzene	77	[69]
Naphthalene	94	[69]
Tetracene	90	[70]
Pentacene	90	[70]
Graphite	118	[69]

Red push the temperature into a range, in which one would expect roughly equal numbers of free and clustered molecules assuming a typical helium-molecule binding energy of 100 cm^{-1}.

Since the equilibrium dimer population depends strongly on the binding energy, our analysis of the equilibrium conditions within the cell would change if the binding energy differed significantly from 100 cm^{-1}. If the helium-molecule binding energy was 77 cm^{-1} (the calculated He-Benzene binding energy [69]) instead of 100 cm^{-1}, the expected equilibrium dimer population at 7K would drop to 20% of molecules from 90%. The dispersed fluorescence of trans-Stilbene-He clusters place an upper bound of 82 cm^{-1} for the trans-Stilbene-He clusters in the electronic excited state [58]. Only a few helium-molecule binding energies have been measured or calculated in the ground electronic state. Table 3.1 lists calculated helium-molecule binding energies for benzene, graphite and several polycyclic aromatic hydrocarbons. Based on the range of binding energies, an estimate of 100 cm^{-1} is a reasonable assumption for molecules with multiple aromatic rings.

We are limited in our ability to directly measure the temperature of the molecules in our setup because the light source used for detection is relatively broadband. The acquired spectra confirm that molecules are at a temperature below 40 K, but more

Table 3.2: Typical cell temperatures during experimental operation.

molecule	temp range (K)	typ. temp (K)
Benzonitrile	5.6–6.6	6
trans-Stilbene	6.1–7.1	6.5
Nile Red	7.2–7.5	7.5

precise temperature information is required to understand if conditions favor dimer formation. In a very similar cell, FTMW spectroscopy has confirmed that molecules are approximately 7 K and are generally within less than 1 K of the temperature of the cell walls, under similar cell wall temperatures and flow conditions [41]. Based on this data, we assume that cell conditions would favor dimer formation in equilibrium.

As an additional check, we can model the temperature increase in the buffer gas due to a heat load using a heat transfer simulation package in COMSOL [71]. In this simulation, we assume that the entire heat is deposited into the buffer gas at a distance of 1 cm from the cell walls. Even with a heat load of 0.5 Watts on the buffer gas, the buffer gas temperature rises only 0.3 K in one of the detection regions. Figure 3.2 shows the temperature gradient of the buffer gas in the cell for an applied heat load of 0.2 Watts and helium density of 2×10^{14} cm^{-3}. Figure 3.3 shows the temperature of the cell along the cell center line (x = 0). The two vertical bars mark the 'upstream' and 'downstream' detection regions. These simulations indicate the even with a heat load of 0.5 W (larger than the 0.4 W heat load measured from the cryostat cold time), the buffer gas temperature should rise less than 0.3 K and stay low enough to favor dimer formation in equilibrium conditions.

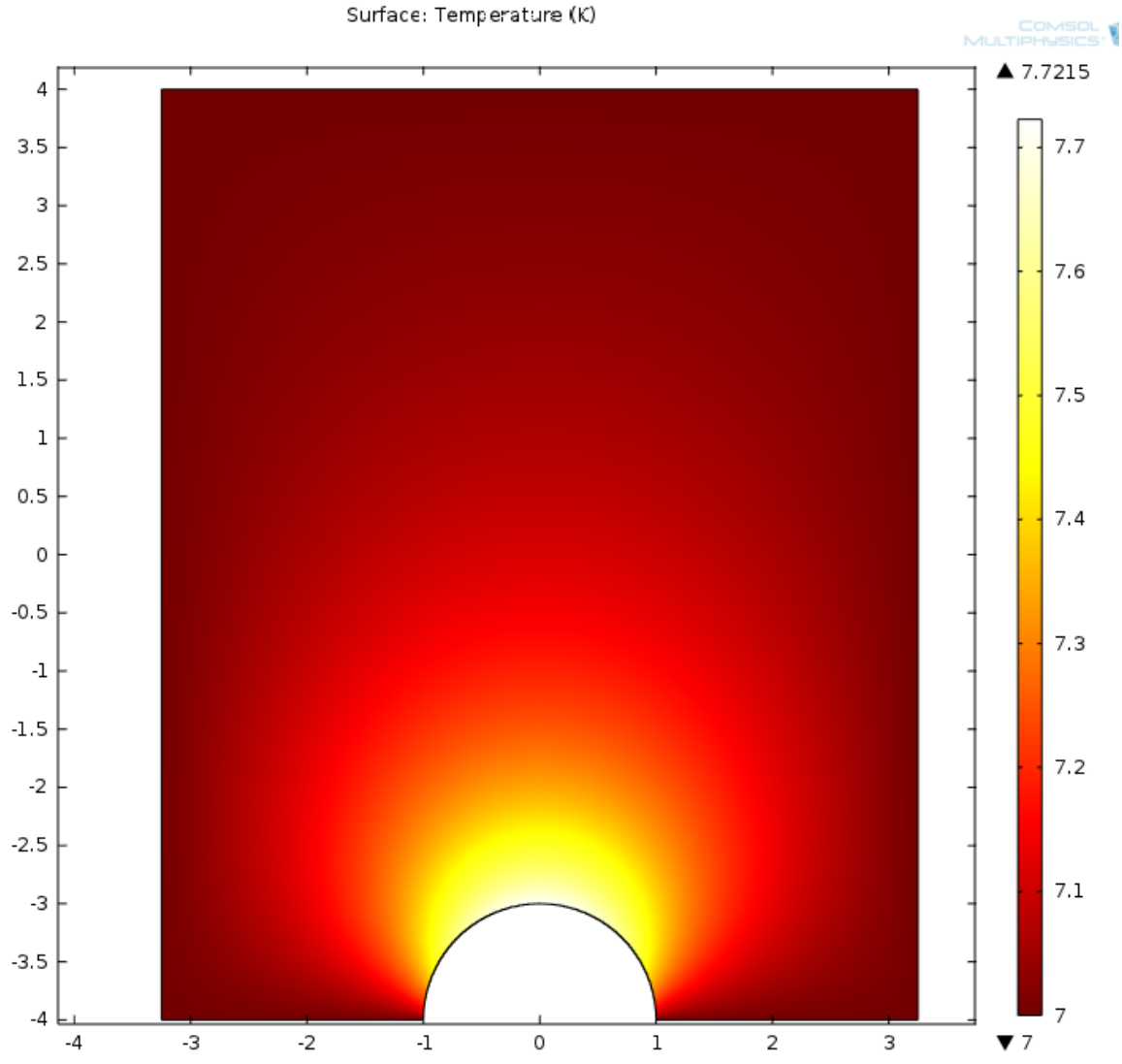

Figure 3.2: Temperature gradient seen in helium buffer gas for a heat load of 0.2 W as simulated with the COMSOL simulation package.

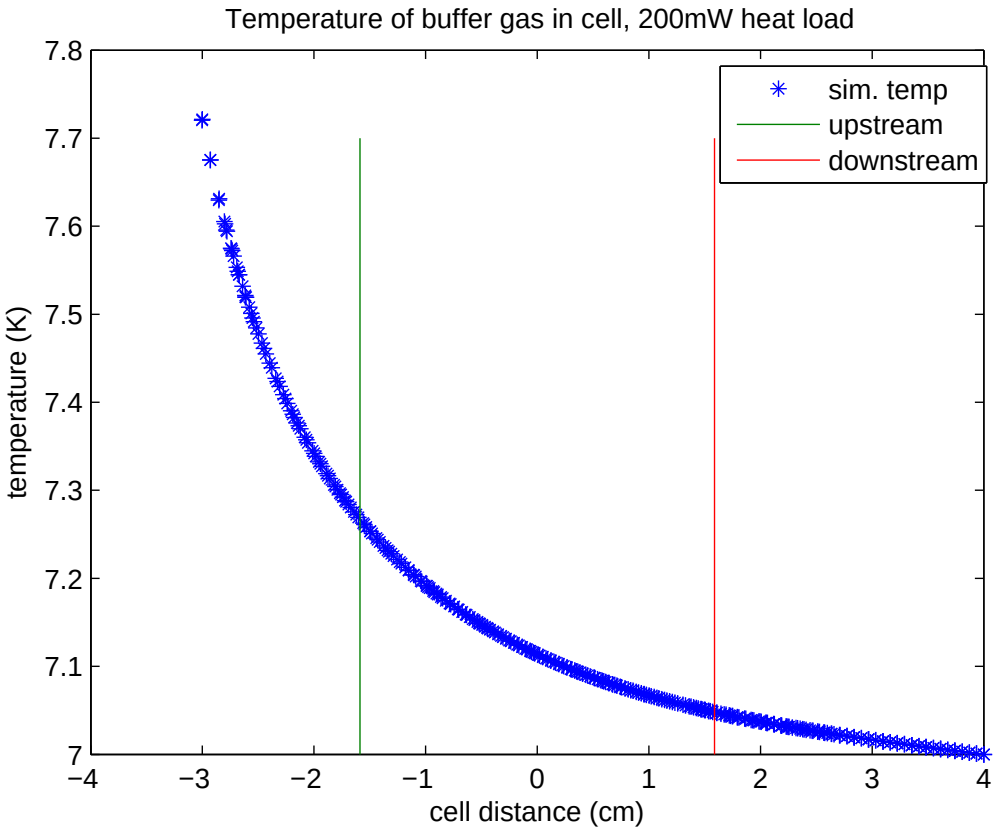

Figure 3.3: Temperature profile of helium buffer gas along the cell center line. The two vertical lines mark the locations of the two detection regions in the cell.

3.2 Cluster formation

Pioneered by Frank de Lucia [17] and our group [34], buffer gas cooling now has been shown to produce large, dense, cold samples of small polyatomic molecules, but it's unknown how 'large' a molecule can be cooled in this way. In particular, buffer gas atoms may start to stick to the molecules during the cooling process, forming small clusters. More generally, it is unknown which molecular properties will lead to sticking, and the residence time as a function of specific internal structure is unknown. In strong supersonic expansions, van der Waals clusters between molecules and the carrier gas atoms routinely form at relatively high temperatures ($\sim$100 K) [50], possibly through three-body collisions. But, evidence of van der Waals clusters in buffer gas cooled systems has only been observed at temperatures below 1 Kelvin [72, 73].

Stable cluster formation requires three bodies to satisfy conservation of energy and momentum and may proceed either directly via three body recombination or through the Lindemann mechanism [47], as shown in figure 3.4. In the latter case, a molecule and a helium atom form a short lived collision complex. When the residence time of the helium-molecule complex exceeds the mean time between helium collisions, fully bound helium-molecule clusters can form, in a 'delayed three body' reaction. In low temperature He-CO collisions, the complex lifetime is measured to be 10^{-10}s [74].

3.2.1 Role of molecular structure in complex lifetimes

The internal structure of a molecule will determine collision residence times, but the detailed relationship is unknown. Vibrational and rotational modes will certainly

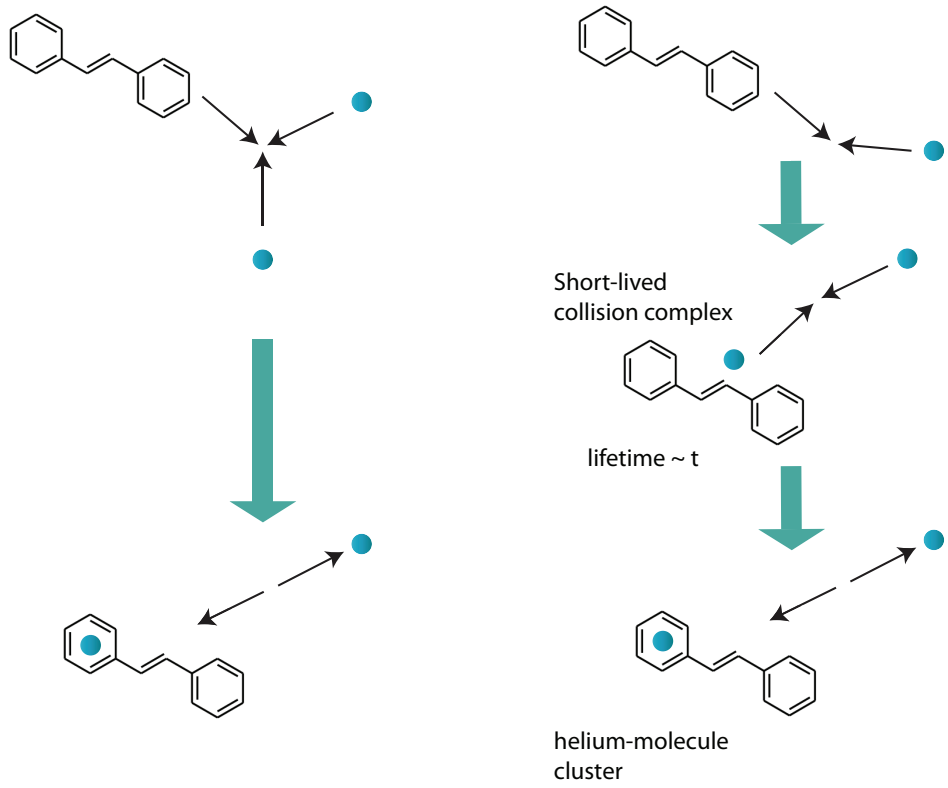

Figure 3.4: Cluster formation requires three bodies to conserve energy and momentum. It may proceed either directly through three body recombination or through a resonant process, the Lindemann mechanism.

play a role in determining the lifetime of the collision complex [48, 49]; additional atoms can lead to a larger number of modes with smaller energy spacings, leading to longer lifetimes. Amongst polyatomic molecules, there's a wide range in the energies of the lowest vibrational mode above the ground state, depending significantly on the molecule's structure (as opposed to only the number of atoms). 'Rigid' molecules, such as C_{60} and Benzonitrile, can have lowest energy vibrational mode spacing upwards of 150 cm^{-1} [75] while 'floppy' molecules, such as trans-Stilbene, can have low energy torsional mode spacings less than 10 cm^{-1} [76]. This can be compared to the He-molecule binding energy, typically 100 cm^{-1}; the binding energy can excite many of the torsional modes but few or none of the vibrational modes. Figure 3.5 shows a comparison of density of available vibrational states for a 'rigid' and 'floppy' molecule.

One model of collision complexes suggests that molecules with vibrational modes comparable in energy to the available energy in a helium molecule collision could form longer lived complexes with helium, indicating, generally, that floppy molecules may be more prone to clustering with helium than rigid ones [34]. Previous work within our group demonstrated buffer gas cooling of relatively rigid naphthalene and Fluorobenzene with no signs of buffer gas-molecule cluster formation [34, 41]. Here, we explore the buffer gas cooling of a very floppy molecule, trans-Stilbene and a much larger molecule, Nile Red, which is of a size similar to many human hormones. We again observe no signs of He-molecule cluster formation. Under the assumption of molecular cooling to the cell temperature, this allows us to place limits on the lifetime of He–trans-Stilbene clusters created in two-body collisions in this system.

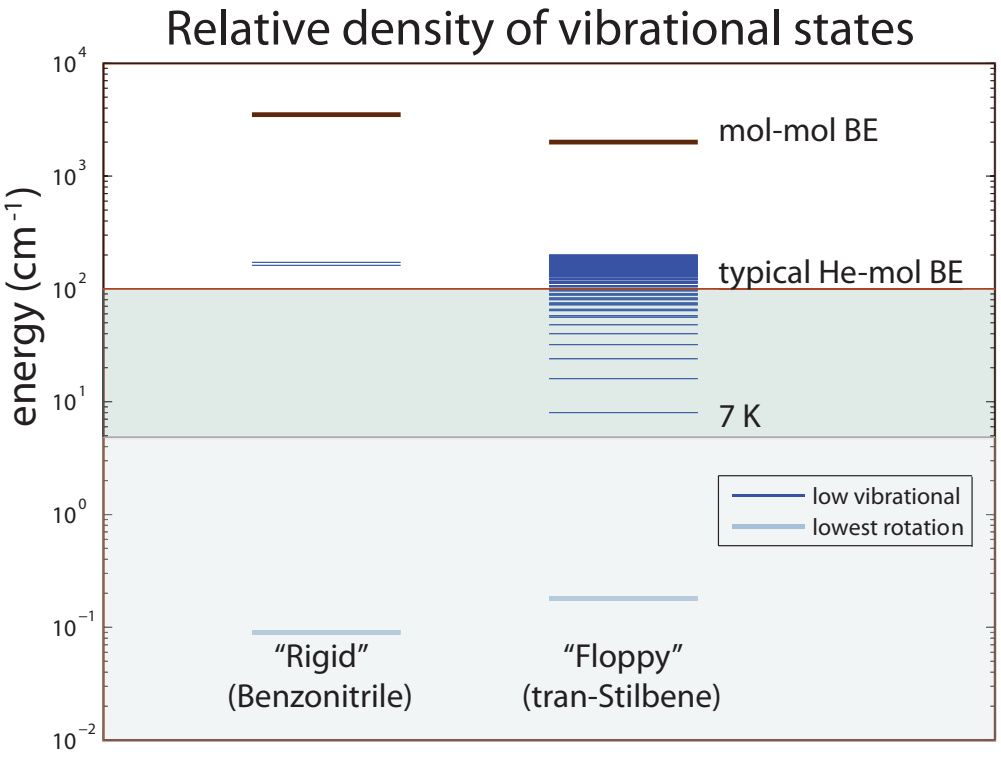

Figure 3.5: A comparison of the relative number of accessible states for a 'rigid' and 'floppy' molecule. The lightly shaded region represents the typical collision energy, and the darker shaded region shows the states available to the collision complex. Only vibrational states with an energy less than 200 cm^{-1} are shown.

3.2.2 Theoretical calculation of a collision-complex lifetime

When an atom and molecule collide and form a short-lived collision complex, the entire binding energy of the atom to the molecule becomes available for exciting rotational and vibrational states of a molecule. As a result, the collision partners in a complex may be found in any combination of internal states provided that the combined energy of the pair does not exceed the binding and translational energy. In collisions involving polyatomic molecules, the first reaction that forms a collision complex limits the rate of all subsequent reactions, and the Lindemann mechanism best describes the dynamics [47].

In a theoretical paper, Croft and Bohn propose that Rice-Ramsperger-Kassel-Marcus (RRKM) approximation is appropriate for such collisions and that the collision complex lifetime τ may then be estimated from the density of rovibrational states available within the collision ρ and the number of channels by which collision fragments may exit the complex N_0:

$$\tau = \frac{2\pi\hbar\rho}{N_0}[49].$$

When an atom and molecule collide, the pair may be in any combination of rovibrationally excited states with an energies less than the binding energy and energy of the individual collision partners. However, an atom and molecule can only separate when the pair are in the relatively few states accessible by the energy of the collision partners. During a collision, the pair explores the phase space of states available until they find an exit channel. Larger binding energies result in longer complex lifetimes. In order to have collision complex lifetimes of 1 μs or longer required for observation of cluster formation in low density buffer gas cells, the number of states available to

the collision complex would need to be approximately 100,000 times the number of states, in which a molecule may exit the complex.

3.3 Results

3.3.1 Helium – trans-Stilbene cluster lifetime

The UV spectroscopy of both trans-Stilbene ($C_{14}H_{12}$) and clusters of trans-Stilbene–He (TS-He) has been previously well characterized in supersonic jets [58, 77]. The molecule has been well studied in the chemistry community because it can be converted between cis and trans isomers with UV light [78]. Trans-Stilbene has a torsional mode with an energy of 8 cm^{-1} [76], an energy comparable to that available in a typical trans-Stilbene–He collision. In a simple model of the Lindemann mechanism, as proposed in ref [34], the low energy torsion modes of trans-Stilbene could give rise to a longer collision complex lifetime, allowing for enhanced cluster formation with helium. Buffer gas cooling of trans-Stilbene provides insight into how the lowest vibrational modes may influence a collision complex lifetime and whether very floppy molecules may be cooled using buffer gases. A LIF spectrum of buffer gas cooled trans-Stilbene is shown in figure 3.6. The electronic origin and several low frequency vibrational modes of the excited state are prominent.

When trans-Stilbene forms a van der Waals cluster with helium, the electronic zero-zero transition red shifts by 5.8 cm^{-1} per helium atom [58], which is larger than the typical 2-3 cm^{-1} shifts seen for van der Waals clusters of helium with other molecules [14]. Each trans-Stilbene may cluster with up to four helium atoms, and the

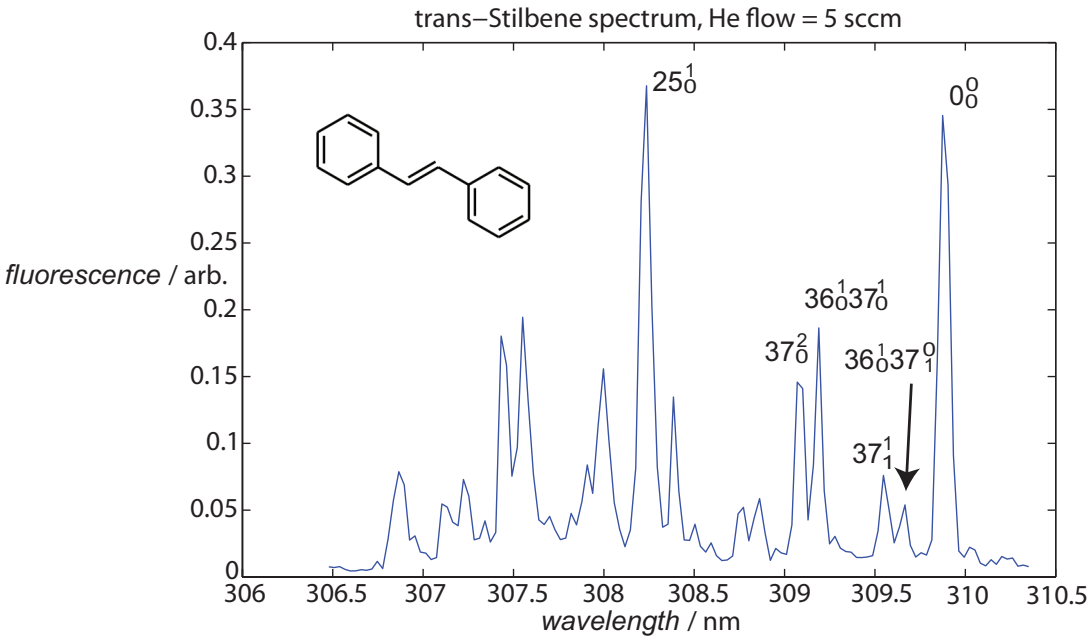

Figure 3.6: LIF spectrum of cold trans-Stilbene taken with a helium buffer gas flow of 5 sccm. The electronic origin and several low frequency modes of the excited state are prominent.

atoms may stick on both sides of the two phenyl groups [58]. Larger TS-He clusters have never been observed experimentally.

Since the 5.8 cm^{-1} shift is less than the 7 cm^{-1} linewidth of the OPO used for detection, our detection method cannot individually resolve cluster peaks, yet the OPO linewidth is small enough to reveal any significant population of TS-He clusters through line asymmetry. In our data, we observe a highly symmetric zero-zero line under all experimental conditions, in particular for all helium flow rates and for cell temperatures of 6.5–7 K, as shown in figure 3.7. From those data, we can place an upper bound on the population of TS-He clusters of 5% of the trans-Stilbene in the cell. Since the equilibrium population favors cluster formation at temperatures equal to or less than 7 K, the lifetime of the trans-Stilbene-helium collision complex can be inferred to be shorter than the mean time between helium collisions in the cell, approximately 50 μs. Successful buffer gas cooling of trans-Stilbene suggests that the technique should also work for other molecules, even those with similar low lying vibrational states, in particular those with vibrational energy spacings less than the collision or helium-molecule binding energy.

3.3.2 Nile Red

Comprised of 42 atoms, Nile Red ($C_{20}H_{18}N_2O_2$) is much larger than any other molecule previously buffer gas cooled and is very comparable in size to many important human hormones. We chose Nile Red for the tests in this apparatus because many other similar sized molecules either thermally decompose or require higher oven temperatures than is feasible in our current apparatus; enthalpy studies of Nile Red

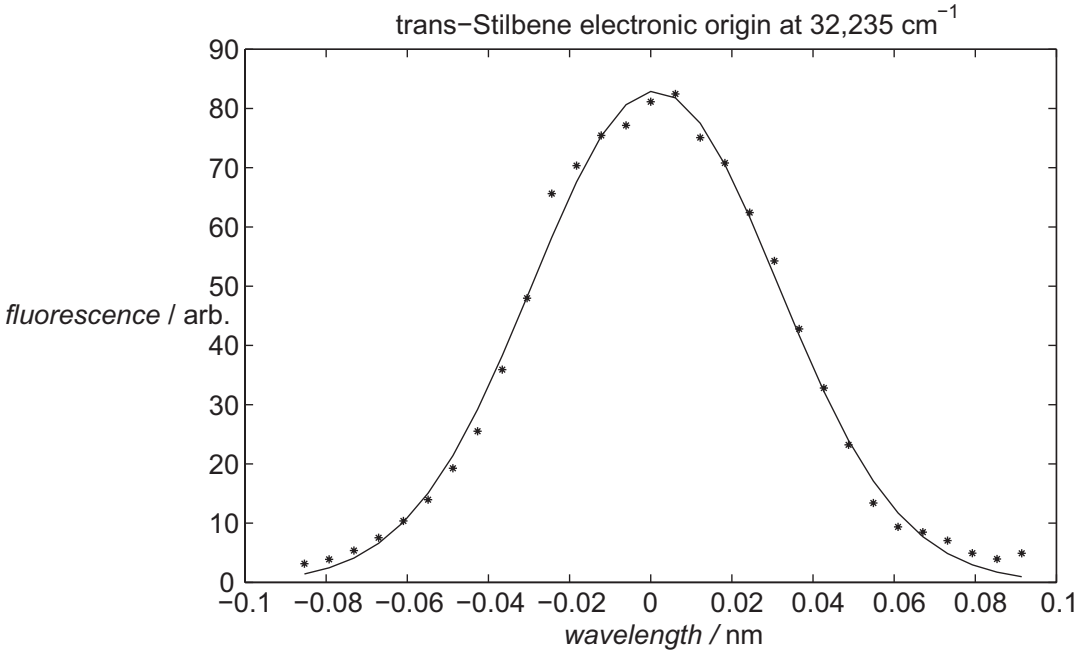

Figure 3.7: Electronic origin of trans-Stilbene with a Gaussian curve fit. No signs of asymmetry were observed at any helium flow rates indicating a lack of helium - trans-Stilbene cluster formation in the cell above the 5% level.

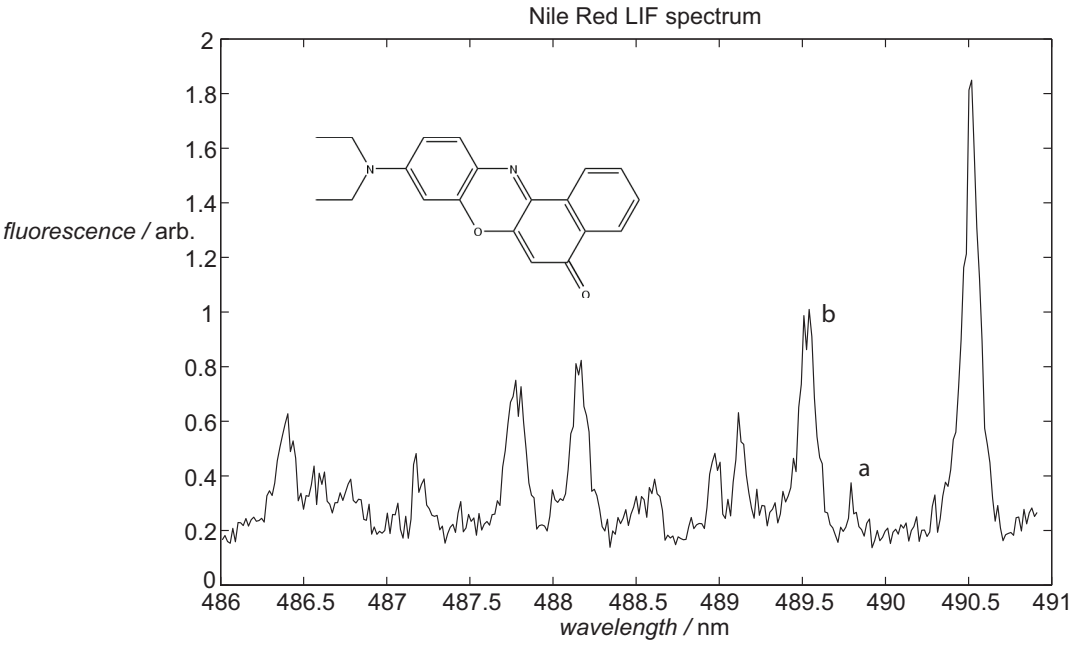

Figure 3.8: LIF spectrum of Nile red in a cold buffer gas cell. Labels a and b indicate lines with tentative assignments.

(NR) indicated a significant vapor pressure of Nile Red at or around 480 Kelvin [79]. Nile Red is a dye used to stain intercellular lipid droplets for detection via fluorescence microscopy [80].

Although the Nile Red absorption and fluorescence spectrum have been well characterized in solution [81], the gas phase spectrum is previously unreported. The wavelengths that Nile Red absorbs and fluoresces in solution depend strongly on the polarity of the solvent. (Nile Red has an estimated dipole moment of 8.4 Debye based on solvatochromatic studies [82].) Generally, the spectra of molecules in non-polar solvents such as cyclohexane tend to more closely match gas phase spectra; a peak absorption at 488 nm in cyclohexane and a calculated gas phase electronic origin at 488 nm [83] prompted a search for lines in the 510–475 nm range.

Table 3.3: Observed lines in Nile Red spectrum

wavelength (nm)	relative shift (cm^{-1})	tentative assignment
490.52	0	main transition
489.79	30	wag
489.54	41	OOP bend
489.12	58	
488.97	64	
488.61	80	
488.17	98	
487.78	115	
487.17	140	
486.40	172	

The gas phase fluorescence spectrum of cold Nile Red is shown in figure 3.8, and a list of observed lines appears in table 3.3. A strong line at 490.5 nm starts a series, and no additional lines were observed to the red of the spectrum, up to 510 nm. Several lines are observed within 2 nm of the strongest line. These may be low energy torsional modes of the excited state [84]. Low level calculations in Gaussian [1] of Nile Red indicate that there are four excited vibrational modes with energies below 100 cm^{-1}. We tentatively assign the first peak, labeled a in figure 3.8 and located at 30 cm^{-1} from the origin, to correspond to out of plane waving of the diethylamino group. A second peak labeled b at 41 cm^{-1} may correspond to an out of plane bending motion of the molecule. The close spacing of the lines and density of calculated vibrational modes combined with the relatively broad linewidth of the OPO limit our ability to further assign any lines in the spectrum.

Alternatively, some lines in the spectrum may be hot bands that have not fully cooled in the buffer gas, as seen in buffer gas cooling of other molecules [85]. In supersonic beams, hot bands are identified by monitoring a spectrum for line amplitudes

that decrease with up to 50 fold increases in the backing pressure of the carrier gas [13]. In the system used in these experiments, the in-cell helium density may only be varied by a factor of 5, limiting the ability to identify hot bands using a similar method. However, with modest increases of the helium flow, no lines changed intensity relative to the strongest line. This is consistent with the lines arising from either low energy vibrational modes of the electronic excited state or hot bands with small inelastic vibrational quenching cross sections.

Tentative line assignment based on calculations with Gaussian.

We can use Gaussian, a program for modeling electronic structure of molecules, to estimate the vibrational modes of a given molecule. Gaussian is a versatile tool used within the Chemistry community to understand molecular structures, spectra and reactions. For simple molecules, such as Benzonitrile, low level calculations of vibrational modes take about 15 minutes and accurately describe the vibrational motion. Energy predictions for vibrations are typically within about 10 cm^{-1} for low energy modes. Calculations for molecules as complicated as Nile Red take approximately half a day. Here we use the DFT B3YLP with a basis set of 3-21g to optimize the molecular geometry and estimate the vibrational modes for the ground state of Nile Red. The results are shown table 3.4.

Comparing the calculations to the acquired LIF spectra, we find that the first two calculated electronically excited state frequencies are near the values for the first two measured peaks. Since the predicted third vibrational mode falls at nearly twice the frequency of the first observed peak, it's impossible to assign the remaining

Table 3.4: Calculated ground state vibrational modes for two conformers of Nile Red

Vibrational Mode	Conformer 1 (cm^{-1})	Conformer 2 (cm^{-1})
1	26	27
2	38	31
3	60	63
4	81	89
5	95	126

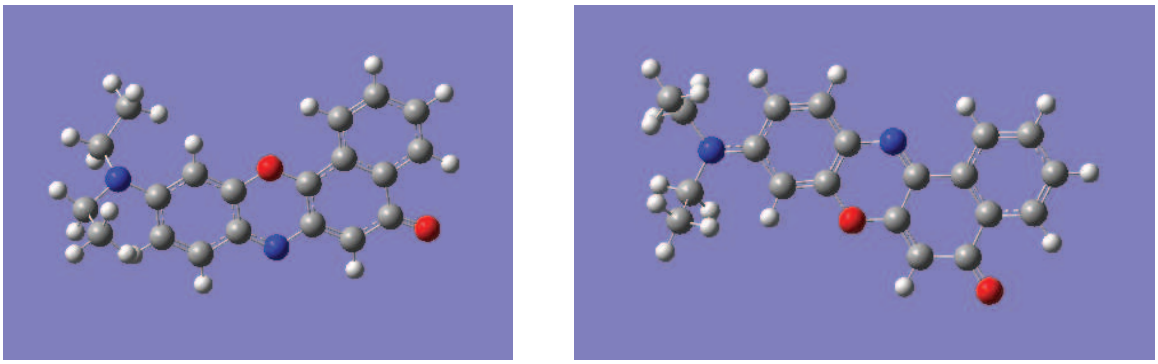

Figure 3.9: Two conformers as optimized by Gaussview. Vibrational modes for the first conformer provide a better match to the observed spectra.

peaks given the low resolution arising from the broad linewith of the light source. The relatively high density of predicted of low energy vibrational modes also limits our ability to identify progressions and combination lines within the spectra. For vibrations with relatively harmonic potentials, one expects to observe higher harmonic lines at frequencies that are multiples of the fundamental frequency. Observation of lines at predicted locations provides evidence in support of line assignments in a spectrum.

In the spectra of Nile Red, we see sharp lines on a flat background level that is elevated from the overall background due to scatter light, which can be seen in figure 3.10. Since we observe a very little scattered light in presence of molecular flow without helium flow, small wiggles in the background between 486.5–487 nm and other regions suggest that there may be some weaker, unresolved lines in the spectrum. Some of the lines in the spectrum, in particular the line at 488.61 nm, are wider than others, indicating that multiple lines may overlap in this region. Spectroscopy of Nile Red with a narrower band light source would aid in the identification of lines.

Spectroscopists often rely on more data than just the LIF spectra when assigning lines. For instance, dispersed fluorescence spectra for each prominent peak often provides information on the frequency components within a transition, helping to identify which vibrations may be involved in the transition [77]. Other techniques, such as spectral hole burning, can also provide further insight into the conformers and clusters of molecules. Unfortunately, we did not have these capabilities in this apparatus.

Possible observation of Nile Red dimers

We observe that a combination of molecular and buffer gas flow resulted in an elevated fluorescence level for the entire fluorescence spectrum shown in figure 3.10. One might attribute the elevated baseline to overall broadband molecular fluorescence. At higher molecular flow rates (higher oven temperatures), the level of the elevated fluorescence baseline at 491 nm rises, and the broad fluorescence feature rises further at shorter wavelengths as measured at both the upstream and downstream observation regions. The strength of this feature increases with increasing molecular flow rates (higher oven temperatures). At intermediate molecular flow rates, a broad spectral feature appears in the spectrum measured downstream that is absent in the upstream spectrum, as shown in figure 3.10.

Since the broad feature appears at higher molecule flow rates, we suggest that it may be explained by the formation of molecular (NR-NR) dimers [86]. Molecules undergo collisions with helium and potentially other Nile Red molecules while traveling between the upstream and downstream observation points. While the molecule-helium and molecule-molecule cross sections are unknown, molecule-molecule cross sections are generally larger than than molecule-helium cross sections. As discussed in the apparatus section, we calculate that 5 percent of Nile Red molecules collide with other molecules. Other molecules are known to rapidly form dimers during molecule-molecule collisions, and Nile Red likely behaves the same. For example, under similar flow conditions, we have directly observed Benzonitrile dimers forming under similar conditions [85]. While dimers of some molecules exhibit narrow spectral features, many molecular dimers, including naphthalene, have broad LIF spectra [87].

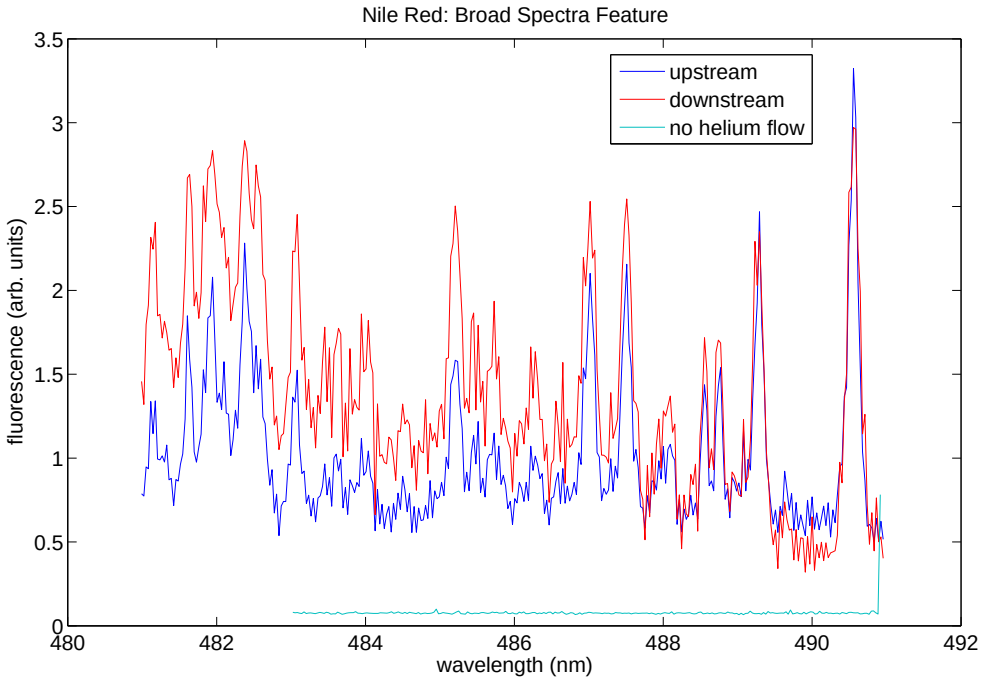

Figure 3.10: Higher molecule flow rates resulted in the appearance of a broad spectral feature consistent with the formation of molecular dimers. At an intermediate molecule flow rate shown here, a broad spectral feature appeared in a spectrum taken at the downstream detection point while simultaneously no such feature was observed upstream. A third trace shows the background scatter observed without helium gas flow.

The appearance of a broad spectral feature at higher Nile Red flow rates is consistent with the formation of NR-NR dimers in the cell.

No evidence of Nile Red-helium clusters

No asymmetry was observed in the strong transition at 490.5 nm for any helium flows suggesting no signs of molecule-helium cluster formation. Due to the higher heat loads on the cell from a higher oven operation temperature, the temperature of the cell rose to 7.5 K, a temperature where a mix of clustered and free molecules

would be expected in equilibrium. Because there are no theoretical predictions for the spectral shift of NR-He clusters, it's not possible to place an upper bound on the fraction of NR-He clusters (and therefore any bound on NR-He lifetimes). If a single adhered helium atom resulted in a 5.8 cm^{-1} light shift (as is the case for TS-He clusters), an upper bound of 10% of NR in clusters would result from our data.

3.4 Conclusion

We observe buffer gas cooling of a floppy molecule, trans-Stilbene, and a large molecule, Nile Red, in a 7 K buffer gas. We report evidence of no trans-Stilbene–He cluster formation, placing an upper bound of 5% on the population of He–trans-Stilbene in the cold buffer gas. Also, a cold gas phase spectrum of Nile Red is reported for the first time. In addition to narrow spectral features, we also observe a broad spectral feature at higher molecule flow rates, which is suggestive of molecule-molecule clustering. These results show that it is possible to buffer gas cool into the Kelvin regime non-rigid and small biological sized molecules with many internal degrees of freedom. Extension to other similar and larger molecules should be explored for applications ranging from chemical studies to mixture analysis.

Chapter 4

Vibrational relaxation cross sections and molecular dimers

Benzonitrile molecules are cooled through collisions with cold (6K) helium buffer gas and are studied using optical spectroscopy. Measurements of Benzonitrile vibrational state decay results in determination of the vibrational relaxation cross sections of $\sigma_{22} = 8{\times}10^{-15}$ cm^2 and $\sigma_{21} = 6{\times}10^{-15}$ cm^2 for the 22 (v=1) and 21 (v=1) states. We also report the first direct observation of cold molecular dimers in a cryogenic buffer gas cell and determine the dimer formation cross section to be $\sim 10^{-13}$ cm^2.

4.1 Introduction

In recent years, ever larger and more complex molecules have been cooled in supersonic jet expansions [13, 14, 15]. Spectroscopy of biological molecules in such jets has lead to the characterization of different conformers [22]. Further studies could

enhance the understanding of structure in biological systems [21]. Cluster formation has also been studied in such beams, and many large molecules form clusters in supersonic expansions with high stagnation pressures; van der Waals clusters and molecule-molecule dimers have been studied [88, 50].

Buffer gas methods offer a complimentary approach to the cooling of molecules, the study of collisions and determination of molecular structure. As discussed in Chapter 3, recent experimental developments have extended buffer gas cooling to significantly larger molecules. In contrast to the rapidly varying collision environment found in supersonic expansions, the gas cooling collisions occur in a (cold) rarefied buffer gas environment, essentially eliminating direct three body collisions.

Previous work on buffer gas cooling of naphthalene inferred the creation of naphthalene-naphthalene (N-N) dimers through an effective two body process. This was done in experiments measuring molecule loss rates in a buffer gas flow tube with high helium densities [34]. We now report the first direct observation of cold molecular dimers in a lower density buffer gas (without flow). We study their formation, definitively identifying the two-body nature of their dimer formation.

The relatively uniform density environment present in our buffer gas cell is also excellent for measuring helium-molecule relaxation cross sections. Three regimes describe the dependence of vibrational relaxation cross sections on small variations in the temperature. At the lowest temperatures (significantly colder than temperatures in this experiment), relaxation collisions occur in the Wigner regime where s-waves dominate. In this case, relaxation cross sections approach a constant that depends on the scattering length of a molecule's rovibrational state [89].

At temperatures similar in energy to the van der Waals binding energy of two collision partners, vibrational quenching rate coefficients reach a minimum value and rise at either lower or higher temperatures. The temperature corresponding to the minimum quenching rate increases for collision pairs with larger van der Waals binding energies [89]. On finer temperature scales within the van der Waals regime, contributions from partial waves with nonzero angular momentum give rise to shape resonances and enhancements in quenching rate coefficients [89]. In the case of ^{4}He-CO collisions, the van der Waals interaction potential is deeper than the potential for He-H_2, and more shape resonances are observed in the quenching coefficients [89]. Theoretical calculations compare well with the results from He-CO and He-H_2S pressure broadening cross sections measured in cryogenic buffer gas cells, using millimeter wave absorption spectroscopy [17, 74, 89]. In the van der Waals regime, the potential may also support Feshbach resonances arising from couplings between bound and unbound channels [89] and exhibits quantum effects. Finally, vibrational quenching rate coefficients rise for higher temperatures [89].

We also report here the measurement of the vibrational relaxation cross sections for the 21 (v=1) and 22 (v=1) states of Benzonitrile in collisions with atomic helium at low temperature. While similar measurements of this type are possible in supersonic jets, there are fewer cold collisions in jets, and the interpretation of jet data requires complex modeling of collisions throughout the expansion [90]. The relatively uniform density environment present in our buffer gas cell is excellent for measuring helium-molecule relaxation cross sections and the study of molecular dimers.

4.2 Apparatus

Our experimental approach employs a cryogenic buffer gas to cool molecules; molecules from a 300K source flow through an aperture and then into a cold (6 K) cell, which is filled with helium buffer gas. The cell and oven geometry are nearly identical to that described in ref [41]. A hot 0.5 cm diameter oven line is separated from a cell by about 2 cm, so as to reduce the radiation heat load on the cell, thus allowing operation at oven temperatures as high as 500 K. Aluminized mylar is wrapped around the oven line to further reduce the radiative heat load on the cell. Molecules flow through a 1.25 cm hole in the side of a cold 6.5 cm x 6.5 cm x 8 cm aluminum cell, which is attached to a helium bath. Helium gas flows through a cold 0.2 cm diameter copper fill line into an annular manifold around the aperture of the cell, filling the cell with cold helium buffer gas and forming a 'curtain' at the aperture. The typical mean time between molecule-helium collisions in the cell is about 50 microseconds. [1]

As hot molecules flow from the oven toward the cell aperture, they collide with cold helium buffer gas atoms that continually exits the cell. Simulations estimate that about 20% of the 1 $\times 10^{18}$ molecules $\cdot$ s^{-1} flowing from the oven reach the cell interior [41]. Once inside the cell, molecules are estimated to undergo about 100 elastic collisions before reaching the cell walls, a process that takes a few milliseconds. Benzonitrile molecules require about 50 collisions with cold helium to cool translationally and rotationally to the temperature of the buffer gas [41]. Typical helium flow rates used in these experiments vary between 2–9 sccm [2] and correspond to an

[1] Here was assume an elastic cross section of 3×10^{-14} cm^2 [41].

[2] A standard cubic centimeter per minute corresponds to a flow of approximately 4.5 $\times 10^{17}$ atoms per second.

estimated He density of 1–5 $\times 10^{14}$ cm^{-3} $\pm$ 1 $\times 10^{14}$ cm^{-3}. In two different regions of the cell, separated by 3.2 cm, molecules are detected via laser induced fluorescence at 260–275 nm with light from a doubled Optical Parametric Oscillator (OPO) as shown in figure 1. Between the two detection regions, molecules collide with approximately 50 cold helium atoms, and a small fraction collide with other molecules. Based on the geometry of the copper line and measured pressure in the oven, we estimate that typical molecule flow rates are about 3 sccm, corresponding to an calculated in-cell molecular density of 2 $\times 10^{12}$ cm^{-3} $\pm$ 1$\times 10^{12}$ cm^{-3}. While helium-Benzonitrile and Benzonitrile-Benzonitrile collision cross sections have not previously been measured, we can conservatively estimate that they are similar to or greater than rotational relaxation cross sections for other similar molecules, about 3-5$\times 10^{-14}$ cm^2 [41]. From this, we estimate the time between molecule-molecule collisions is approximately 10 ms, and that approximately 5% of molecules in the cell collide with other molecules before reaching the cell walls (under our typical molecule flow conditions).

4.3 Results

We observe the laser induced fluorescence spectra of Benzonitrile on the $S_0 \rightarrow S_1$ transition in the region of 260-275 nm, including two hot bands (21_1^1 and 22_1^1) and the dimer electronic origin, as shown in figure 4.1. Molecular spectra are observed in the 'upstream' and 'downstream' regions (locations shown in figure 2.1). Vibrational relaxation cross sections for helium-molecule collisions are measured by comparing the two spectra, as explained below. We also observe Benzonitrile dimers form in the buffer gas through molecule-molecule two body collisions.

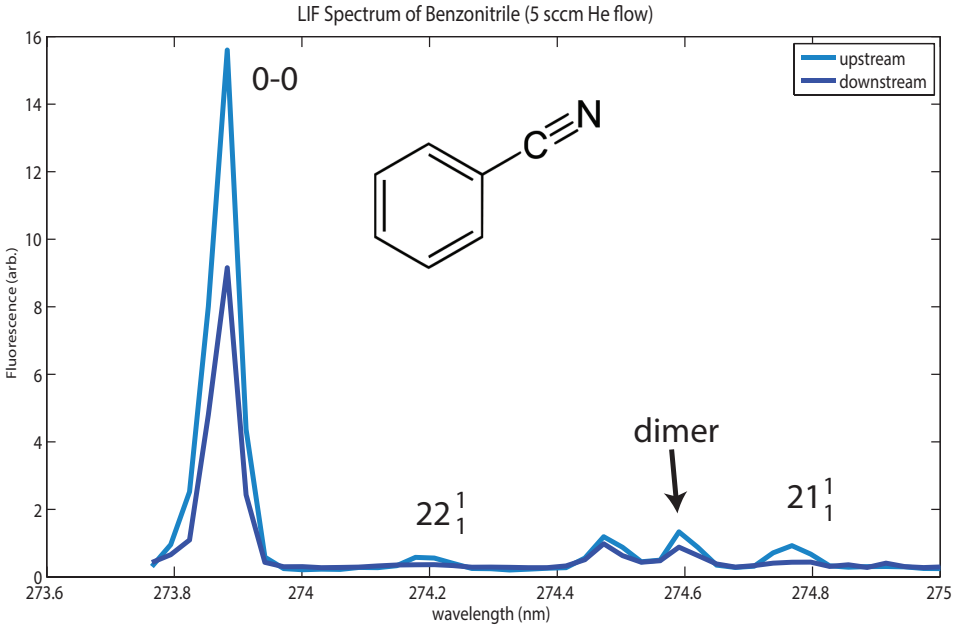

Figure 4.1: Benzonitrile spectrum at both upstream and downstream points at 5 sccm helium and 3 sccm Benzonitrile flow. From left to right, we observe the electronic origin for the monomer at 273.88 nm, the 22^1_1 transition, probably the 22^2_2 transition or an artifact, the dimer electronic origin and the 21^1_1 transition.

4.3.1 Vibrational relaxation cross sections

The observed hot bands 21_1^1 and 22_1^1 correspond to an out-of-plane C-N bending mode and an out-of-plane C-C-N deformation respectively [86, 91, 92]. As molecules undergo collisions with cold helium atoms between the upstream and downstream detection points, the population in the excited 21 (v=1) and 22 (v=1) vibrational modes decreases relative to the population of molecules in the ground state under some molecule and helium flow conditions. The relative signals for the two states in the 'downstream' region are $\frac{1}{3}$ and $\frac{1}{2}$ of the relative signals in the 'upstream' region, respectively. The number of state changing collisions N is determined by the molecular mean free path λ, the distance between measurements d, the helium density n and the vibrational relaxation cross section σ_{vib} as follows:

$$N = \frac{d^2}{4\lambda^2} = \frac{n^2\sigma_{vib}^2 d^2}{2}$$

From the data, we measure vibrational relaxation cross sections of 8×10^{-15} cm^2 $\pm$ 2×10^{-15} cm^2 and 6×10^{-15} cm^2 $\pm$ 2×10^{-15} cm^2 for 22 and 21 states respectively. The cross sections are accurate within 30 percent, and the largest uncertainty in the cross section comes from the estimated helium density inside the cell. These cross sections are similar to the largest vibrational relaxation cross sections previously measured for Fluorobenzene in ref [41] (see table 1). The Fluorobenzene modes are now identified as the in-plane (IP) mode 18b (a), the out-of-plane (OOP) mode 16a (b), and the out-of-plane mode 11 (c) [93]. Helium-molecule vibrational relaxation cross sections for both molecules are at least an order of magnitude less than typical helium-molecule rotational relaxation cross sections [41].

The cross sections for all measured out-of-plane deformations are larger than the

Table 4.1: Vibrational relaxation cross sections for Benzonitrile and Fluorobenzene

Molecule	Mode #	Type	σ_{vib}	Ref
Benzonitrile	21	OOP	6×10^{-15} cm^2	this work
Benzonitrile	22	OOP	8×10^{-15} cm^2	this work
Fluorobenzene	18b	IP	1×10^{-16} cm^2	[41]
Fluorobenzene	16a	OOP	4×10^{-16} cm^2	[41]
Fluorobenzene	11	OOP	3×10^{-15} cm^2	[41]

one measured in-plane deformation of Fluorobenzene, and our measurements on Benzonitrile suggest that, generally, out-of-plane modes may have higher vibrational relaxation cross sections than in-plane modes in other substituted benzene rings as well. Intuitively, this makes sense because a vibrational quench of an in-plane helium mode could require an edge on collision with the ring while helium collisions with the face of a ring could result in an out of plane vibrational quench. Classically, a cross section of a ring face is larger than a cross section of a ring side.

4.3.2 Benzonitrile dimers

We observe cold Benzonitrile dimers in the cold buffer gas. The spectroscopy of the Benzonitrile dimer has been previously well characterized in supersonic beams [86, 94], where dimers form in the intermediate density and temperature regime of the supersonic expansion. The electronic origin of the dimer was observed to be red shifted 92 cm^{-1} from the electronic origin of the monomer [86]. The dipole-dipole interaction stabilizes the Benzonitrile molecules into a planar configuration [95]. Measurements of the rovibronic spectrum of the Benzonitrile dimer indicated that the lowest intermolecular vibration is an out-of-plane butterfly mode with an energy of 10.3 cm^{-1} [95]. Two other intermolecular vibrational modes, an out-of-

plane twisting mode and an in-plane gearing mode, have energies below 40 cm^{-1} in the ground state [95].

Shown in figure 4.1 is a spectrum of Benzonitrile in the buffer gas cell revealing a cold peak at 274.60 nm, the wavelength of the dimer zero-zero transition. This peak increases with the square of the Benzonitrile flow, which correlates with the in cell Benzonitrile density, as shown in figure 4.2, indicating that dimer formation occurs in an environment where molecules undergo collisions with cold helium. Based on the geometry of the cell and a curve fit to these data, we estimate a dimer formation cross section of $(2\pm2)\times10^{-13}$ cm^2. At both the upstream and downstream measurement points, the ratio of the dimer to monomer signal remains about 0.1 for moderate helium (3-4 sccm) and molecule flow conditions, suggesting that dimers are quite stable while undergoing collisions with cold helium atoms, not accumulating helium atoms, through multiple sticking events. An analysis analogous to the method outlined in the previous section of this paper places an upper bound of 3 $\times10^{-15}$ cm^2 on cross section for dissociation of dimers due to collisions with helium.

Estimate of the Benzonitrile dimer binding energy

Although the Benzonitrile-Benzonitrile binding energy is not known, we can roughly estimate the energy of the dipole-dipole interaction stabilizing the dimer from measured geometries and molecular properties. Benzonitrile has a dipole moment of 4.48 Debye [96], which is considerably larger than the dipole moment of a typical diatomic molecule [86]. Its molecular dimer is known to be held in a planar configuration by the attractive interaction of the two dipoles as shown in figure 4.2 with an intermolecular

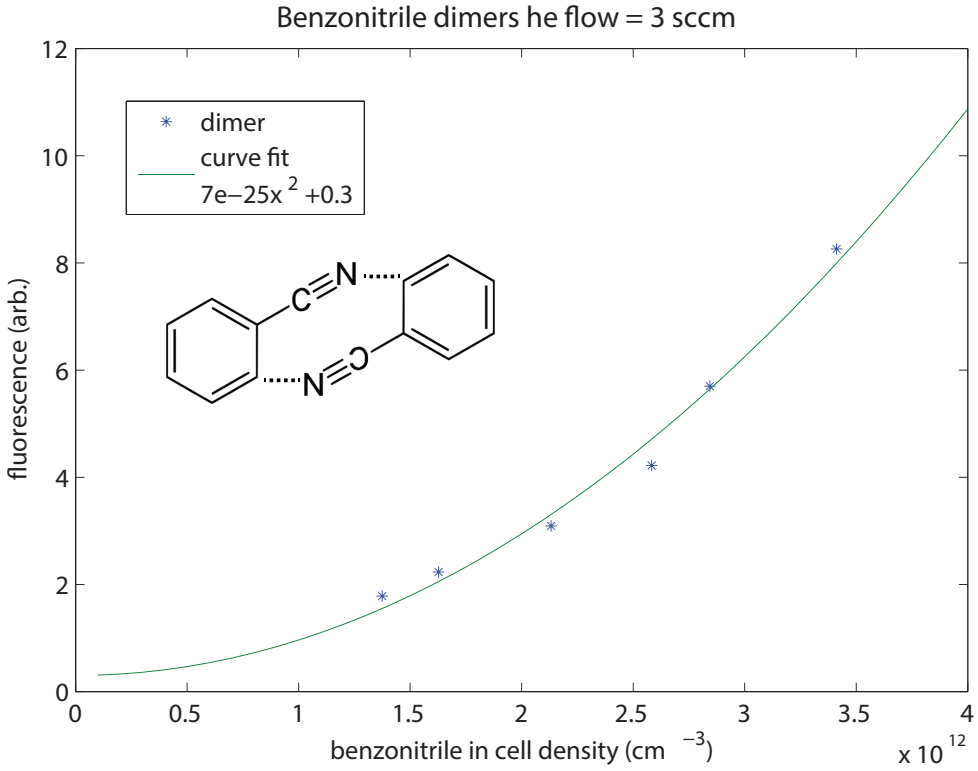

Figure 4.2: Benzonitrile dimer signal increases with the square of Benzonitrile flow in the apparatus. Data was taken at a helium flow rate of 3 sccm and cell temperature of 6.7 K.

spacing in the dimer is 2.9 angstroms [86]. The energy U of two interacting dipoles with moments μ at a separation of r is given by

$$U = \frac{1}{2\pi\epsilon_0}\frac{\mu^2}{r^3}$$

where ϵ_0 is the permittivity of free space. Given the molecular dipole moment and intermolecular spacing, the interaction energy for the two dipoles is approximately 3500 cm^{-1}. This value is consistent with the range of 2500-8000 cm^{-1} for typical binding energies for dimers bound by dispersive and weak electrostatic forces [56]. For comparison, dimers held by van der Waals forces, including helium-molecule dimers, tend to have binding energies less than 2500 cm^{-1}[56].

4.4 Conclusion

For the first time, cold molecular dimers are observed in a cold buffer gas cell and seen to form with a molecule-molecule formation cross section of $(2\pm2)\times10^{-13}$ cm^2. With several low energy intermolecular vibrational modes, the Benzonitrile dimer is one of the least rigid systems ever buffer gas cooled, and successful buffer gas cooling of Benzonitrile dimers, as well as molecules with low lying vibrational modes of similar energies [97], suggests that cooling of other similarly non-rigid molecules, including biological molecules, is feasible. In contrast to the varying conditions of a supersonic expansion, the buffer gas has significantly more uniform temperature and density, and these conditions allow for straight forward measurements of vibrational relaxation cross sections of large molecules. Relaxation cross sections for two out-of-plane vibrations of Benzonitrile are measured and found to be similar to those

measured for similar out-of-plane vibrations in Fluorobenzene.

Chapter 5

Applications and future directions

5.1 Buffer gas cooling of even larger molecules

Since we observe no evidence of helium-molecule cluster formation for trans-Stilbene and Nile Red, one direction of study is to continue to pursuing the limits of buffer gas cooling for large polyatomic molecules. By comparing the features of the molecules studied in this work, we can identify properties that may lead to helium-molecule sticking and select molecules that may form helium-molecule clusters in this system.

5.1.1 Comparison of available vibrational states in molecules studied

In this work, we saw evidence for no clustering of helium with trans-Stilbene, Nile Red, Benzonitrile or Benzonitrile molecular dimers in a cold buffer gas cell. However, we did observe formation of Benzonitrile-Benzonitrile dimers, which indicates the

complex lifetime for two Benzonitrile molecules is longer than 1 μs. We can compare the relative number of vibrational states available to the complex for each of these molecules, as shown in table 5.1, to see if we can gain some insight into how many available states a complex would need to form dimers in this system.

While available vibrational states are expected to play an important role in a complex lifetime, there is disagreement over the role of rotational states in determining the residence time [48, 68, 34]. Many rotational states are energetically accessible during helium-molecule collision, yet one paper suggests that conservation of angular moment constrains the rotational states available to the complex [34]. Since rotational relaxation collisions are known to occur (in fact, buffer gas cooling of molecules works because of efficient quenching of rotational states), molecules may exit the complex in other rotational states.

For the case of helium-molecule dimers, any vibrational states with energies less the combined total of the binding energy and translational energy can be excited in a complex. 'Rigid molecules', such as Benzonitrile whose lowest vibrational mode is 146 cm^{-1}, have no available vibrational excited states with energies below the typical helium-molecule binding energy of $\sim$100 cm^{-1}. In contrast, trans-Stilbene has three vibrational modes with energies less than the binding energy, for a combined total of 23 available vibrational states. The three available modes are a ν_{37} phenyl torsional mode at 8 cm^{-1}, ν_{36} phenyl flap mode at 58 cm^{-1} and ν_{72} phenyl wag mode at 76 cm^{-1} [98]. A nice illustration of the physical motion of all three modes can be found in the same ref [98].

Since the binding energy of Benzonitrile molecular dimers is over an order of

Table 5.1: Available states and estimated binding energies for various clusters.

cluster	available vib. states	estimated binding energy (cm^{-1})	Ref
He-TS	23	100	[98]
He-B	1	100	[92]
He-NR	8	unknown	[1]
B-B	5600	3500	[92]
(B-B)-He	55	100	[95]

magnitude greater than the typical helium-molecule binding energy, many more vibrational states are available to the complex, potentially resulting in a longer lifetime as discussed in Section 2 of Chapter 3. In addition, the presence of two molecules allows for combinations of vibrational states, leading to a larger phase space for the complex in comparison to atom-molecule complexes. Assuming a binding energy of 3500 cm^{-1} for the Benzonitrile-Benzonitrile complex, a conservative estimate places the number of available states at 5600, two orders of magnitude higher than the available vibrational states for a complex of helium and a floppy molecule.

Based on this comparison, we would estimate that a molecule with thousands of vibrational states below the helium-molecule binding energy would be likely to cluster with helium in a cell at these temperatures and densities, assuming a helium-molecule binding energy of 100 cm^{-1}. In all of the molecules studied in this thesis, the translational energy available to the molecules is less than the energy of the lowest lying vibrational states, so molecules may only exit the complex in the ground vibrational state. For a molecule with several thousand vibrational states with energies below 100 cm^{-1}, some states would likely have energies less than $\sim$7 cm^{-1} and consequently, also be available exit channels, reducing a complex lifetime.

5.1.2 Candidate molecules

If our goal is to further investigate the role of vibrational states in the onset of helium cluster formation, working with molecules that have on the order of hundreds of vibrational or hindered rotational states below 100 cm^{-1} would be a nice place to start. Unfortunately, a lack of a centralized database for spectroscopy data makes finding such molecules in the literature challenging. Torsional motions of phenyl (benzene rings) and methyl groups (carbon with three hydrogens) tend to have very low energies [99]. Searching for molecules cooled in supersonic jets with these functional groups is a nice starting point for finding molecules with many accessible energy states below typical helium-molecule binding energies.

As it turns out, trans-Stilbene is probably one of the most spectroscopically studied molecules with low lying vibrational states, and as such, it is an excellent choice of molecule for studying helium-molecule cluster formation in a buffer gas cell. The presence of a phenyl group at the end of a chain seems to allow for a wider range of low energy vibrations. Only m-Xylene comes close to having the same number of internal levels less than 100 cm^{-1} with 18 available energy levels, and a brief discussion of inconclusive results of buffer gas cooling of Xylenes appears in Appendix 1.

In reviewing the literature on spectroscopy of large molecules in supersonic jets, one molecule Zinc Tetraphenylporhine (ZnTTP) stands out both for its size (678 amu) and number of available torsional modes [100]. Its structure, as well as the structures of all candidate molecules discussed, is shown in figure 5.1, and table 5.2 compares properties of all candidate molecules . With four phenyl groups, ZnTTP has a number of low energy states. Unlike many molecules of a similar size, its electronic

Table 5.2: Candidate molecules further clustering studies.

molecule	available vib. states	temp (K)	atoms	mass (amu)	ref
ZnTTP	4	653	77	678	[100]
PM567	22	348	48	318.22	[1]
8-PhPM	17	348	31	267.8	[1]
9-PA	5	393	34	254.3	[101]

spectroscopy is well characterized, providing a nice frame work for interpreting any acquired spectra. ZnTTP also readily transfers into the gas phase upon heating although it requires higher oven temperatures than the existing apparatus can handle.

Several other molecules with less well characterized spectroscopy look promising based on their spectroscopic behavior in supersonic beams and helium nanodroplets. In a supersonic beam, two pyromethene dyes 1,3,5,7,8-pentamethyl-2,6-diethylpyrromethenediuoroborat (PM567) and 8-phenylpyrromethenediuoroborat (8-PhPM) have many low energy spectral lines [102]. A quick glance at the spectra acquired in supersonic beams for both molecules suggests a richer molecular structure than trans-Stilbene. Although the spectral lines have not been identified for either molecule, PM567 has a very congested spectra with many possible van der Waals peaks or low frequency vibrational lines [103]. Either explanation for the spectral features makes PM567 a promising candidate molecule for studying clustering in a cold, low density buffer gas system.

Low level calculations in Gaussian [1], similar to the calculations on Nile Red, suggest that both molecules have many low energy vibrational modes. These calculations do not include hindered rotations within the molecule. Since the presence of multiple methyl groups within a molecule tends to give rise to hindered rotations and

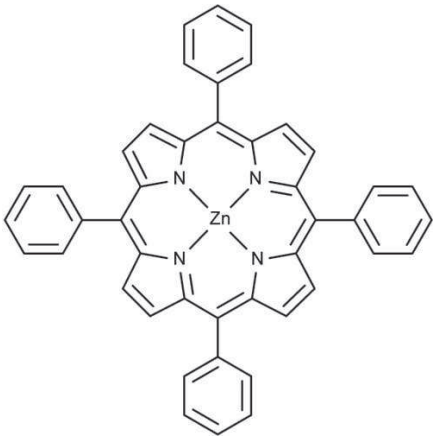

ZnTTP

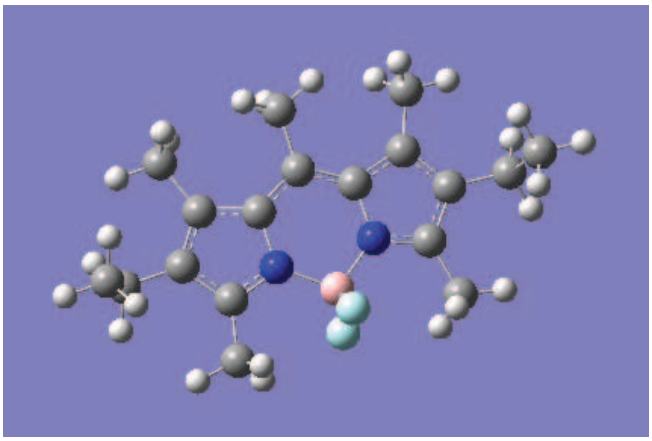

PM567

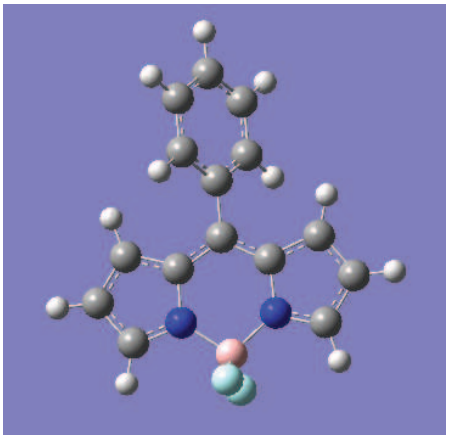

8-PhPM

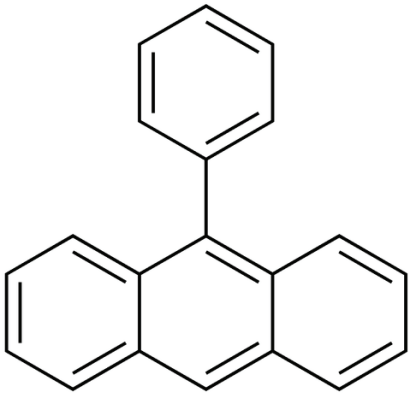

9-PA

Figure 5.1: Lewis structures and three dimension representations of candidate molecules. Three dimensional representations were created with a combination of Gaussview 5 and Gaussian [1].

small splittings, the number of estimated available states is likely underestimated for PM567.

In general, ref [102] suggests that molecules with more congested spectra in supersonic beams may exhibit broader spectral features in nanodroplets, indicating a greater interaction with the helium droplet. It's also possible that such molecules may also be more prone to clustering. A fourth molecule, 9-phenylanthracene (9-PA), has a number of accessible vibrational states below typical helium-molecule binding energies and better characterized spectroscopy [101]. 9-phenylanthracene also exhibits broad features in helium nanodroplets [102]. If cluster formation was extensive enough to allow the formation of helium nanodroplets around the cold molecules, the resulting spectra for these molecules would be substantially broadened, limiting the ability to study the molecules spectroscopically in a buffer gas cell. Table 5.2 summarizes some of the known properties of all suggested candidate molecules, and figure 5.1 shows structures of molecules discussed in this section.

5.1.3 Technical considerations for larger molecules

The required oven temperatures for at least one of these species are greater than 500 K, the maximum operation temperature of the existing oven. Typically, larger molecules have lower vapor pressures and require heating to higher temperatures to generate enough gas phase sample. Working with some of these molecules would require either re-engineering of the cell to handle higher heat loads or an alternative method for transferring molecules into the gas phase that places a lower heat load on the cell.

In the current apparatus, we estimate that the heat load on the helium bath is approximately 0.7 W at maximum oven temperatures. The behavior of the sorbs indicates that this is about the maximum heat load that the system can handle before the pumping capacity and speed of the sorbs is compromised, leading to shorter experimental runs and limiting maximum helium flow rates.

Higher cooling power to handle higher heat loads

A pulse tube based system, can provide more cooling power at these temperatures than a helium cryostat. Typical pulse tube systems can provide up to 1.5 W of cooling power at 4.2 Kelvin [104]. Since run times appeared limited by the capacity of the charcoal to store helium at higher temperatures, adding additional sorb area could allow for longer cold times. Sorbs both pump helium faster and have a larger capacity for storing helium at lower temperatures. If one moved to working with molecules that required even higher oven temperatures, the extra cooling power of the pulse tube could help maintain the cell at a temperature where cluster formation is favored in equilibrium conditions.

Laser desorption of large molecules

Laser desorption of molecules from surfaces can successfully transfer a number of thermally labile molecules into the gas phase. Recently, femtosecond laser desorption of several proteins has been demonstrated [105]. Energy deposition during a femtosecond laser pulse occurs at a faster time scale than thermal equilibrium timescales, enabling the intact transfer of large biomolecules, including proteins that often unfold upon heating, into the gas phase. Thermal modes that typically lead to

dissociation are not involved.

This technique relies on non-resonant femtosecond laser pulses with intensities of 10^{13} Wcm^{-2}. The entire process is independent of the electronic structure of the target, making it a general method for transferring molecules into the gas phase. Femtosecond laser desorption is relatively insensitive to target structure and works with thin films, liquids and solid targets.

While the method has only been demonstrated at room temperatures, it has a great deal of promise for working at low temperatures. Nanosecond ablation is routinely used to generate sources of radical and stable atoms and diatomic molecules in buffer gas cells. Both methods deposit similar amounts of heat onto the cell, suggesting that a cryogenic buffer gas cell should be compatible with femtosecond laser desorption in addition to the routinely used nanosecond laser ablation.

Femtosecond laser desorption may be explored through a simple experiment with a nearly closed, buffer gas cell. Since ablation sources typically require higher in-cell helium densities than the densities described in this thesis, it would be best to start with a cell that has an in-cell helium density on the order of 10^{15} cm^{-3}. A cell nearly identical to the cell used in the experiments may be used if the size of the molecule apertures were reduced to permit a higher helium density within the cell at the same flow rate.

A cell could be configured such that a solid sample is situated on the side of the cell opposite a window. After laser desorption, cold molecules may be detected via LIF further downstream in the cell as shown in figure 5.2. Tryptophan would make a good test molecule for this experiment since its LIF spectroscopy has been well character-

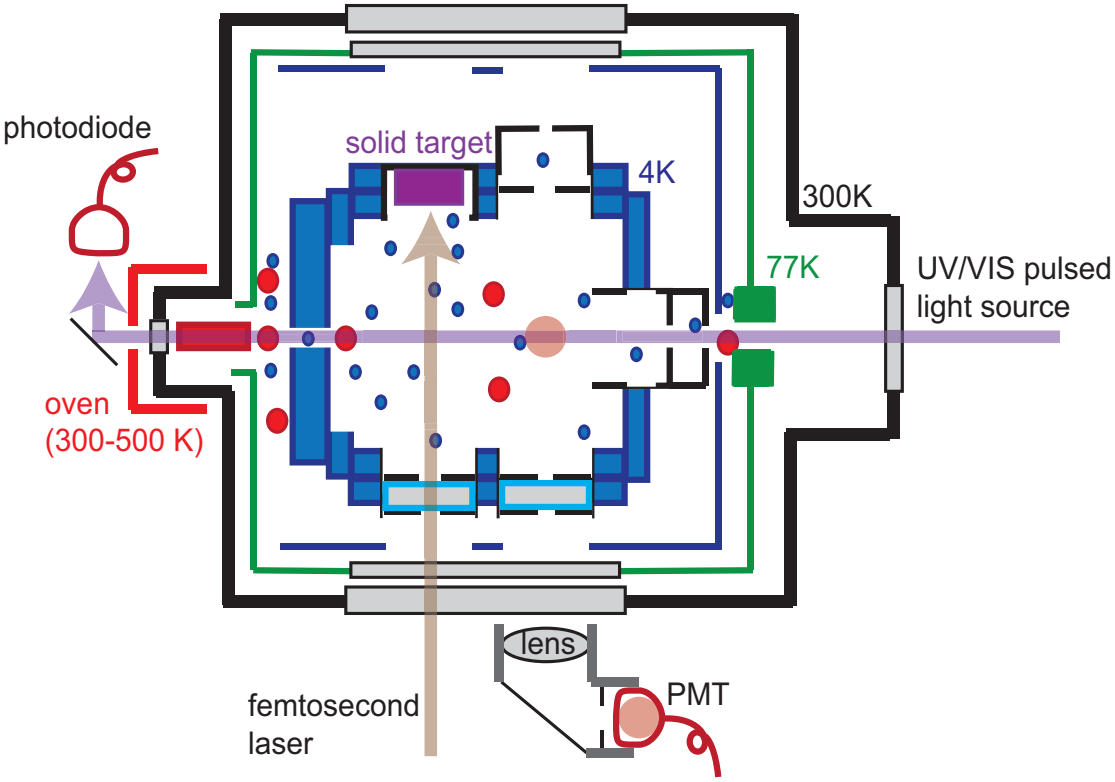

Figure 5.2: An example cell configuration for testing laser desorption of molecules in a cryogenic cell.

ized in supersonic beams [106]. Since it is somewhat thermally labile, oven sources provide relatively low yields of Tryptophan [106]. In contrast to some biomolecules, it is also readily available in powdered form from chemical supply companies. After successful demonstration of laser desorption of a test molecule in a cold, buffer gas filled cell, buffer gas cooling of other biomolecules could be explored.

5.2 Mixture Analysis

The simplified and unique spectra of molecules at low temperatures readily lends itself to identifying components in a complex mixture. Mixture analysis with buffer

gas cooling simply requires that molecules can be transferred into the gas phase, can be buffer gas cooled without significant cluster formation and have known spectroscopy. Many molecules have ultraviolet and visible electronic transitions, yet nearly all molecules have microwave spectra, making microwave spectroscopy a particularly suitable detection option. Buffer gas cooling based mixture analysis has been demonstrated for relatively small polyatomic molecules with UV light and microwaves [20, 18]. Advanced stages of mixture analysis with buffer gas cooling would require building a catalog of spectroscopic data for molecules without previously characterized spectroscopy as has been done for mass spectrometry based mixture analysis systems [27].

Eventually, we may find a molecule, for which significant helium-molecule sticking is observed in a low density cell. While helium-molecule binding energies depend on the molecule, binding energies often fall within a 50 cm^{-1} range, and the relatively small binding energy arises from the low polarizability of helium [64]. The helium-molecule binding energy, temperature and density within the cell set the fraction of free molecules in equilibrium, as discussed in Section 1 of Chapter 3. As a result, the temperature corresponding to a significant onset of cluster formation, should not vary greatly from figure 3.1 for many helium-molecule systems.

Current operational temperatures of and densities in the cell favor helium-molecule cluster formation in equilibrium, yet at a cell temperature of 10 K, most molecules are expected to remain free. The detection scheme described in this thesis cannot distinguish temperatures below 40 K because of the broad linewith of the light source. As a result, raising the cell temperature to 15 K should change the equilibrium conditions

to prefer free molecules without altering the spectral sensitivity. This change should eliminate significant cluster formation and permit the cooling of molecules prone to sticking to the buffer gas.

For microwave detection, the strength of the signal scales as the temperature $T^{-7/2}$ [41]. A rise in temperature from 7 K to 15 K results in a little more than an order of magnitude drop in signal strength. In this case, the performance of mixture analysis in such a cell would suffer, and raising the cell temperature to reduce cluster formation is a less viable option.

Another solution for helium-molecule sticking is to switch to an alternative inert atom for the buffer gas. The atom-molecule binding energy rises with increasing polarizability of the atom, and as a result, the temperature for the onset of equilibrium cluster formation rises as well. Consequently, an atom with a lower polarizability may not form clusters at the same temperatures. Unfortunately, helium has a low polarizability and is already the best choice of atom for avoiding cluster formation. For this reason, helium buffer gas is often chosen as the carrier gas in supersonic beams [61].

5.3 Closing thoughts

The work in this thesis indicates that buffer gas cooling is a robust and versatile method for cooling polyatomic molecules to low temperatures. At this point, we do not see any signs of a fundamental limitation for buffer gas cooling that depend on molecular structure. Technical solutions exist for significant limitations in the capabilities of the current apparatus. Extension of buffer gas cooling to larger molecules,

perhaps biological molecules, holds promise for applications ranging from chemical studies to mixture analysis.

Appendix A

Buffer gas cooling of o-Xylene and p-Xylene

In this appendix, I'll discuss the rather inconclusive results from cooling of ortho-Xylene and para-Xylene. Xylenes are molecules with an aromatic ring with two methyl groups. There are three Xylenes corresponding to the three relative locations of the methyl groups as shown in figure A.1. Ortho-Xylene, meta-Xylene and para-Xylene have many distinguishing properties, including different vapor pressures and UV spectra.

A.1 Hindered rotations in the Xylenes

The relatively proximity of the methyl groups in a xylene strongly influence the internal rotations of the methyl groups within the molecule. In the case of p-Xylene and m-Xylene, time of flight mass spectrometry (TOFMS) and dispersed fluorescence

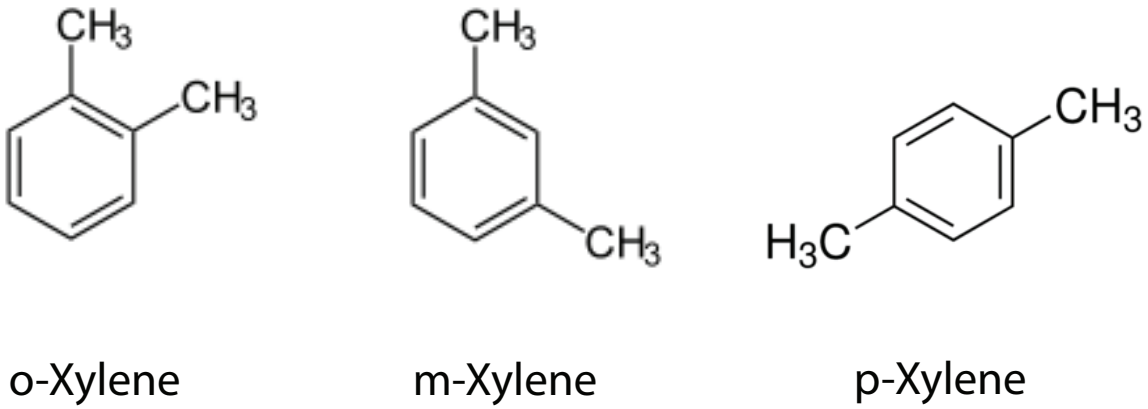

Figure A.1: Lewis structures of the three Xylenes.

Table A.1: Number of internal rotational levels below 100 cm^{-1} [2].

molecule	Number of levels
p-Xylene	18
m-Xylene	16
p-Xylene	1

data indicate that the methyl groups are largely non-interacting, giving rise to a relatively high density of internal rotational levels below 100 cm^{-1} [2]. The close proximity of the two methyl groups in o-Xylene allows for the two methyl rotors to interact and creates a large potential barrier for methyl rotation. As a result of the hindered rotations, o-xylene has far fewer energy levels below 100 cm^{-1} as shown in table A.1 [2].

We have previously suggested that the number of internal molecular states below the helium-molecule binding energy plays a role in the collision complex lifetime. In the case of the Xylenes, the number of energy levels varies by nearly a factor of 20, yet the two molecules have the same number of atoms, are similar in relative size and have nearly the identical structures. All of these features make the Xylenes a nice set

of molecules to study to understand how low energy internal molecular states may affect buffer gas cooling.

A.2 Buffer gas cooling of Xylenes

A.2.1 Data acquisition

The runs for o-Xylene and p-Xylene occurred on different days because the data was acquired at the end of Benzonitrile runs. After completing a set of measurements with Benzonitrile, several mLs of Xylene were injected into the molecule sample region. Since Xylene has a much higher vapor pressure than Benzonitrile, the gas mixture in the sample region was predominately Xylene (85%) as measured by molecular fluorescence for the two measured Xylenes. We also observed a roughly five fold increase in the molecule backing pressure measured in the oven region after the introduction of Xylene. The valves controlling the flow of molecules into the oven region were tuned such that molecule backing pressure was reduced to the same pressure as during the Benzonitrile run. To account for any differences in the apparatus on the two days, we normalize the signal to the Benzonitrile fluorescence signal at the same molecule backing pressure taken minutes earlier.

A.2.2 Observations

Since o-Xylene has fewer internal states, we naively expect to cool more efficiently and likely have a stronger fluorescence signal. Instead, we observe a stronger p-Xylene fluorescence signal relative to the Benzonitrile signal in the cell relative to o-Xylene

Table A.2: Peak molecular fluorescence normalized to Benzonitrile fluorescence

molecule	$\frac{molecule fluorescence}{benzonitrile fluorescence}$
p-Xylene	0.6
o-Xylene	0.2

as summarized in table A.2. One possible explanation for these results is that the oscillator strength for the transition may vary for the Xylenes. Unfortunately, this information was not available in the scientific literature, and we cannot draw any conclusions about this data.

By looking at the peak fluorescence as a function of helium flow, we can understand the optimum conditions for cooling a molecule in our buffer gas cell. A larger fluorescence signal indicates a higher density of cold molecules in the detection region. Since the typical data for molecular fluorescence signal as a function of helium flow has not previously been presented in this thesis, figure A.2 shows the peak signal for the electronic origin of trans-Stilbene as a function of helium flow. This data set shows typical trends the molecular fluorescence as a function of helium flow.

In the upstream region, the largest fluorescence signals occur at moderate helium flows, suggesting that molecules do not fully thermalize at lower flow rates. At higher flow rates, fewer molecules may reach the cell interior due to the a higher density of helium near the entrance to the cell. In the downstream region, fluorescence signals decrease for higher flow rates. The upstream and downstream signals are not normalized to each other. The significantly higher signal levels in the downstream region shown in the figure are an artifact of the significantly higher gain setting for the PMT. PMT gains were adjusted to yield the best spectral data in each region. We observed both smaller molecule signals in the downstream region and less molecular

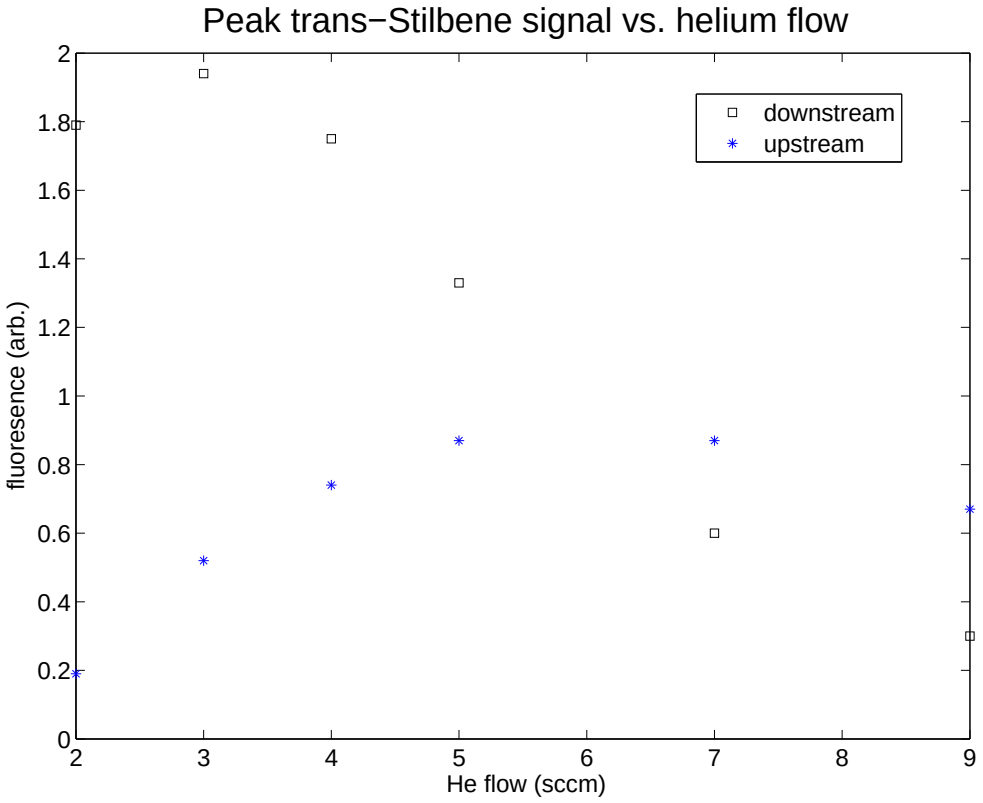

Figure A.2: Peak fluorescence levels for the electronic orgin of trans-Stilbene as a function of helium flow. All data points were taken under the same molecular flows. The observed trends in the magnitude of the signal are typical of that observed in the cooling of other molecules.

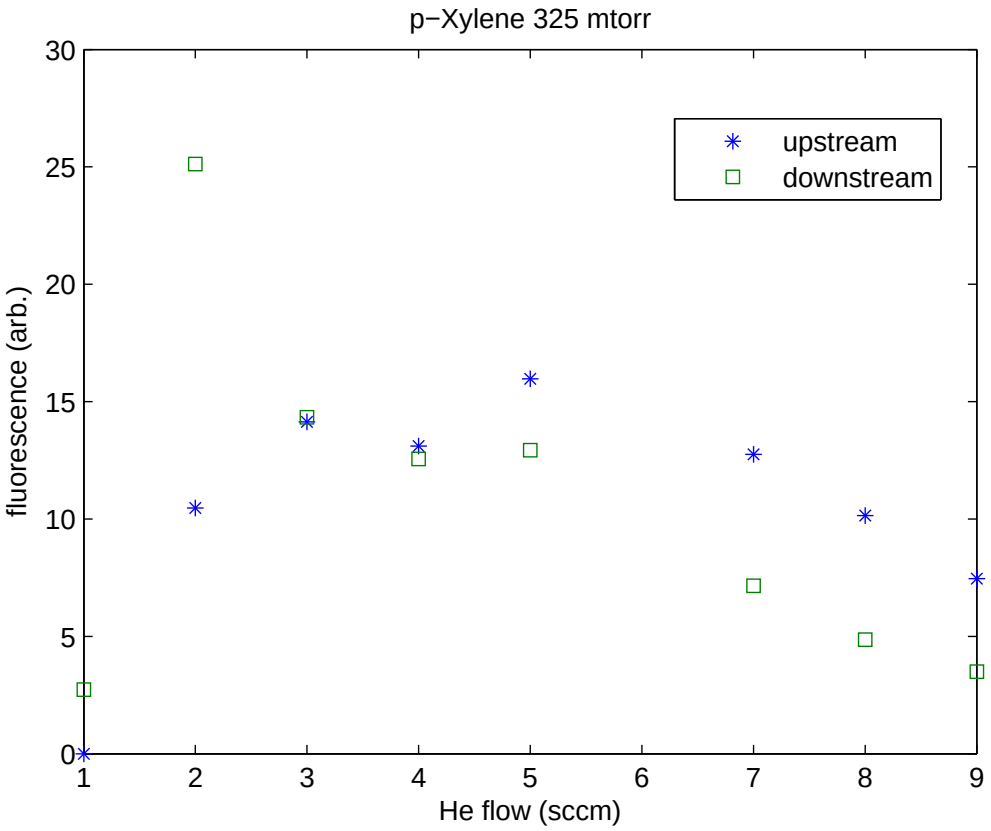

Figure A.3: Fluorescence of the electronic origin of p-Xylene vs helium buffer gas flow.

deposition on the cell during runs as shown in 2.5.

Figures A.4 and A.3 show the peak fluorescence signal from o-Xylene and p-Xylene, respectively. As one can see, the same overall trends are observed in this data as well. The observation of cold molecules in the cell indicates that buffer gas cooling works for Xylenes, but we do not have an explanation for the much smaller fluorescence signal of o-Xylene.

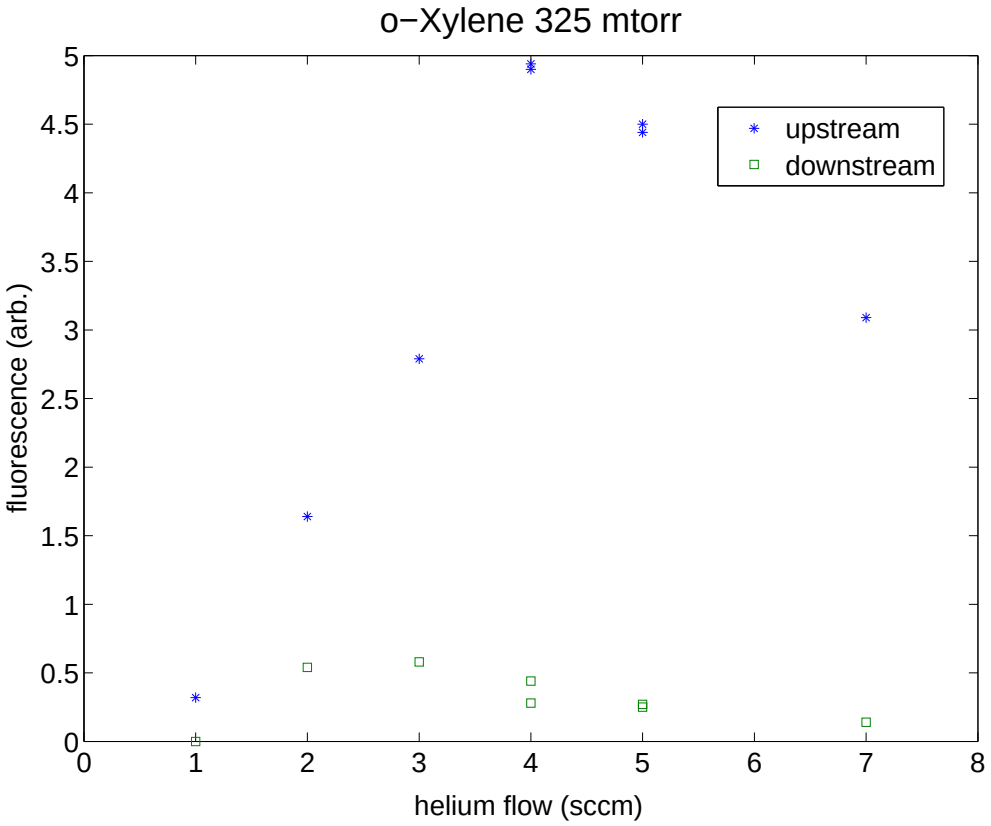

Figure A.4: Fluorescence of the electronic origin of o-Xylene vs helium buffer gas flow.

Bibliography

[1] M. J. Frisch, G. W. Trucks, H. B. Schlegel, G. E. Scuseria, M. A. Robb, J. R. Cheeseman, G. Scalmani, V. Barone, B. Mennucci, G. A. Petersson, H. Nakatsuji, M. Caricato, X. Li, H. P. Hratchian, A. F. Izmaylov, J. Bloino, G. Zheng, J. L. Sonnenberg, M. Hada, M. Ehara, K. Toyota, R. Fukuda, J. Hasegawa, M. Ishida, T. Nakajima, Y. Honda, O. Kitao, H. Nakai, T. Vreven, J. A. Montgomery, Jr., J. E. Peralta, F. Ogliaro, M. Bearpark, J. J. Heyd, E. Brothers, K. N. Kudin, V. N. Staroverov, R. Kobayashi, J. Normand, K. Raghavachari, A. Rendell, J. C. Burant, S. S. Iyengar, J. Tomasi, M. Cossi, N. Rega, J. M. Millam, M. Klene, J. E. Knox, J. B. Cross, V. Bakken, C. Adamo, J. Jaramillo, R. Gomperts, R. E. Stratmann, O. Yazyev, A. J. Austin, R. Cammi, C. Pomelli, J. W. Ochterski, R. L. Martin, K. Morokuma, V. G. Zakrzewski, G. A. Voth, P. Salvador, J. J. Dannenberg, S. Dapprich, A. D. Daniels, . Farkas, J. B. Foresman, J. V. Ortiz, J. Cioslowski, and D. J. Fox. Gaussian 09 Revision D.01. Gaussian Inc. Wallingford CT 2009.

[2] Breem P. J., J. A. Warren, E. R. Berstein, and J. I. Seeman. A study of nonrigid aromatic molecules by supersonic molecular jet spectroscopy. I. Toluene and the xylenes. *J. Chem. Phys.*, 87:1917, 1987.

[3] V. Singh, K. S. Hardman, N. Tariq, M.-J. Lu, A. Ellis, M. J. Morrison, and J. D. Weinstein. Chemical reactions of atomic lithium and molecular calcium monohydride at 1 K. *Phys. Rev. Lett.*, 108:203201, 2012.

[4] M. H. G. de Miranda, A. Chotia, B. Neyenhuis, D. Wang, G. Quéméner, S. Ospelkaus, J. L. Bohn, J. Ye, and D. S. Jin. Controlling the quantum stereodynamics of ultracold bimolecular reactions. *Nat. Phys.*, 7:502, 2011.

[5] K.-K. Ni, S. Ospelkaus, D. Wang, G. Quéméner, B. Neyenhuis, M. H. G. de Miranda, J. L. Bohn, J. Ye, and D. S. Jin. Dipolar collisions of polar molecules in the quantum regime. *Nature*, 464:1324, 2010.

[6] J. Baron, W. C. Campbell, D. DeMille, J. M. Doyle, G. Gabrielse, Y. V. Gurevich, P. W. Hess, N. R. Hutzler, E. Kirilov, I. Kozyryev, B. R. O'Leary, C. D.

Panda, E. S. Petrik, B. Spaun, A. C. Vutha, and A. D. West. Order of magnitude smaller limit on the electric dipole moment of the electron. *Science*, 343:269–272, 2014.

[7] J. J. Hudson, D. M. Kara, I. J. Smallman, B. E. Sauer, M. R. Tarbutt, and E. A. Hinds. Improved measurement of the shape of the electron. *Nature*, 473:493–496, 2011.

[8] L. Carr, D. DeMille, R. V. Krems, and J. Ye. Cold and ultracold molecules: science, technology and applications. *New J. Phys.*, 11:055049, 2009.

[9] D. DeMille. Quantum computation with trapped polar molecules. *Phys. Rev. Lett.*, 88:067901, 2002.

[10] B. Yan, S. A. Moses, B. Gadway, J. P. Covey, K. R. A. Hazzard, A. M. Rey, D. S. Jin, , and J. Ye. Observation of dipolar spin-exchange interactions with lattice-confined polar molecules. *Nature*, 501:521 – 525, 2013.

[11] B. K. Stuhl, M. T. Hummon, M. Yeo, G. Quéméner, J. L. Bohn, and J. Ye. Evaporative cooling of the dipolar radical OH. *Nature*, 492:396, 2012.

[12] S. Schiller and V. Korobov. Tests of time independence of the electron and nuclear masses with ultra cold molecules. *Phys. Rev. A*, 71:032505, 2005.

[13] P. S. H. Fitch, C. A. Haynam, and D. H. Levy. The fluorescence excitation spectrum of free base Phthalocyanine cooled in a supersonic free jet. *J. Chem. Phys.*, 73:1064, 1980.

[14] U. Even, J. Jortner, D. Noy, N. Lavie, and C. Cossart-Magos. Cooling of large molecules below 1 K and He clusters formation. *J. Chem. Phys.*, 112:8068, 2000.

[15] F. Morishima, Y. Inokuchi, and T. Ebata. Laser spectroscopic study of β-estradiol and its monohydrated clusters in a supersonic jet. *J. Phys. Chem. A*, 116:8201–8, 2012.

[16] B. C. Sawyer, B. K. Stuhl, M. Yeo, T. V. Tscherbul, M. T. Hummon, Y. Xia, J. Klos, D. Patterson, J. M. Doyle, and J. Ye. Cold heteromolecular dipolar collisions. *Phys. Chem. Chem. Phys.*, 13:19059–19066, 2011.

[17] D. R. Wiley, D. N. Bittner, and F. C. De Lucia. Pressure broadening cross sections for the H_2S-He system in the temperature region between 4.3 and 1.8 K. *J. Mol. Spectrosc.*, 134:240–242, 1989.

[18] D. Patterson, M. Schnell, and J.M. Doyle. Enantiomer-specific detection of chiral molecules via microwave spectroscopy. *Nature*, 497:475–477, 2013.

[19] V. A. Shubert, D. Schmitz, D. Patterson, J. M. Doyle, and M. Schnell. Identifying enantiomers in mixtures of chiral molecules with broadband microwave spectroscopy. *Angew. Chem. Int. Ed.*, 53:1152–1155, 2014.

[20] D. Patterson. Progress on gas phase cooling and mixture analysis (Harvard case 3670).

[21] J. L. Neill, K. O. Douglass, B. H. Pate, and D. W. Pratt. Next generation techniques in the high resolution spectroscopy of biologically relevant molecules. *Phys. Chem. Chem. Phys.*, 13:7253–7262, 2011.

[22] C. Desfrançois, S. Carles, and J. P. Schermann. Weakly bound clusters of biological interest. *Chem. Rev.*, 100:3943–62, 2000.

[23] M. S. de Vries and P. Hobza. Gas-phase spectroscopy of biomolecular building blocks. *Annu. Rev. Phys. Chem.*, 58:585–612, 2007.

[24] B. K. Stuhl, B. C. Sawyer, M. T. Hummon, and J. Ye. Microwave state transfer and adiabatic dynamics of magnetically trapped polar molecules. *Phys. Rev. A*, 85:033427, 2012.

[25] V. I. Goldanskii. Chemical reactions at very low temperatures. *Ann. Rev. Phys. Chem.*, 27:85–126, 1976.

[26] D. Patterson and J. M. Doyle. Sensitive chiral analysis via microwave three-wave mixing. *Phys. Rev. Lett.*, 111:023008, 2013.

[27] J. A, J. Trygg, J. Gullberg, A. I. Johansson, P. Jonsson, H. Antti, S. L. Marklund, and T. Moritz. Extraction and GC\MS analysis of the human blood plasma metabolome. *Anal. Chem.*, 77:8086 – 94, 2005.

[28] L. P. Parazzoli, N. J. Fitch, P. S. Zuchowski, J. M. Hutson, and H. J. Lewandowski. Large effects of electric fields on atom-molecule collisions at millikelvin temperatures. *Phys. Rev. Lett.*, 106:193201, 2011.

[29] K.-K. Ni, S. Ospelkaus, M. H. G. de Miranda, A. Pe'er, B. Neyenhuis, J. J. Zirbel, S. Kotochigova, P. S. Julienne, D. S. Jin, and J. Ye. A high phase-space-density gas of polar molecules. *Science*, 322:231, 2008.

[30] A. J. Kerman, J. M. Sage, S. Sainis, T. Bergeman, and D. DeMille. Production and state-selective detection of ultracold RbCs molecules. *Phys. Rev. Lett.*, 92:153001, 2004.

[31] J. Küpper, F. Filsinger, and G. Meijer. Manipulating the motion of large neutral molecules. *Faraday Discuss.*, 142:155–173, 2009.

[32] H. L. Bethlem, G Berden, F. M. H. Crompvoets, R. T. Jongma, A. J. A. van Roij, and G. Meijer. Electrostatic trapping of ammonia molecules. *Nature*, 406:491–494, 2000.

[33] D. Patterson, J. Rasmussen, and J.M. Doyle. Intense atomic and molecular beams via neon buffer-gas cooling. *New J. Phys.*, 11:055018, 2009.

[34] D. Patterson, E Tsikita, and J.M. Doyle. Cooling and collisions of large gas phase molecules. *Phys. Chem. Chem. Phys.*, 12:9736–9741, 2010.

[35] N. R. Hutzler, H.-I Lu, and J. M. Doyle. A cryogenic beam of refractory, chemically reactive molecules with expansion cooling. *Chem. Rev.*, 112:4803, 2012.

[36] M. Zeppenfeld, B. G. U. Englert, R. Glöckner, A. Prehn, M. Mielenz, C. Sommer, L. D. van Buuren, M. Motsch, and G. Rempe. Sisyphus cooling of electrically trapped polyatomic molecules. *Nature*, 491:570–573, 2012.

[37] C. B. Connolly, Y. A. Au, E. Chae, T. V. Tscherbul, A. A. Buchachenko, W. Ketterle, and J. M. Doyle. Zeeman relaxation induced by spin-orbit coupling in cold antimony-helium collisions. *Phys. Rev. Lett. A*, 88:021707, 2013.

[38] C. B. Connolly, Y. A. Au, E. Chae, T. V. Tscherbul, A. A. Buchachenko, H.-I Lu, W. Ketterle, and J. M. Doyle. Spin-orbit suppression of cold inelastic collisions of aluminum and helium. *Phys. Rev. Lett.*, 110:173202, 2013.

[39] N. R. Hutzler, M. F. Parsons, Y. V. Gurevich, P. W. Hess, E. Petrik, B. Spaun, A. C. Vutha, D. DeMille, G. Gabrielse, and J. M. Doyle. A cryogenic beam of refractory, chemically reactive molecules with expansion cooling. *Phys. Chem. Chem. Phys.*, 13:18976–18985, 2011.

[40] H.-I Lu, J. Rasmussen, M. J. Wright, D. Patterson, and J. D. Doyle. A cold and slow molecular beam. *Phys. Chem. Chem. Phys.*, 13:18986–18990, 2011.

[41] D. Patterson and J. M. Doyle. Cooling molecules in a cell for FTMW spectroscopy. *Mol. Phys.*, 110:1757–1766, 2012.

[42] W. Campbell and J. M. Doyle. Cooling, trap loading, and beam production using a cryogenic helium buffer gas. In *Cold Molecules: Theory, Experiment, Applications*. CRC Press, 2009.

[43] J. Weinstein. *Magnetic Trapping of Atomic Chromium and Molecular Calcium Monohydride*. PhD thesis, Harvard University, 2002.

[44] M. H. Hummon, T.V. Tscherbul, J. Klos, H.-I Lu, E. Tsikata, W. C. Campbell, A. Dalgarno, and J. M. Doyle. Cold N+NH collisions in a magnetic trap. *Phys. Rev. Lett.*, 106:053201, 2011.

[45] E. Tsikata, W. Campbell, M. Hummon, H.-I Lu, and J. M. Doyle. Magnetic trapping of NH molecules with 20 s lifetimes. *New J. Phys.*, 12:065028, 2010.

[46] J. D. Weinstein, R. deCarvalho, T. Guillet, B. Friedrich, and J. M. Doyle. Magnetic trapping of calcium monohydride molecules at millikelvin temperatures. *Nature*, 395:148–150, 1998.

[47] R. T. Pack, R. B. Walker, and B. K. Kendrick. Three-body collision contributions to recombination and collision-induced dissociation. II. Kinetics. *J. Chem. Phys.*, 109:6714, 1998.

[48] Z. Li and E. J. Heller. Cold collisions of complex polyatomic molecules. *J. Chem. Phys.*, 136:054306, 2012.

[49] J. F. E. Croft and J. L. Bohn. Long-lived complexes and chaos in ultracold molecular collisions. *Phys. Rev. A*, 89:102714, 2014.

[50] A. W. Castleman and R. G. Keesee. Clusters: Properties and formation. *Annu. Rev. Phys. Chem.*, 37:525–550, 1986.

[51] G. Chalasinski and M. M. Szczesniak. Origins of structure and energetics of van der Waals clusters from ab initio calculations. *Chem. Rev.*, 94:17231765, 1994.

[52] K. Nauta and R. E. Miller. Formation of cyclic water hexamer in liquid helium: The smallest piece of ice. *Science*, 287:293–295, 2000.

[53] F. N. Keutsch and R. J. Saykally. Water clusters: untangling the mysteries of the liquid, one molecule at a time. *Proceedings of the National Academy of Sciences of the United States of America*, 98:10533–40, 2001.

[54] B. L. Blaney and G. E. Ewing. Van der Waals molecules. *Ann. Rev. Phys. Chem.*, 27:553–86, 1976.

[55] M. Ito, T. Ebata, and N. Mikami. Laser spectroscopy of large polyatomic molecules in supersonic jets. *Ann. Rev. Phys. Chem.*, 39:123–147, 1988.

[56] H. Pauli. *Atom, Molecule and Cluster Beams I.* Springer, 2000.

[57] Stephen C. Hager, J. W. Laser spectroscopy and photodynamics of Indole and Indole-van der Waals molecules in a supersonic beam. *J. Phys. Chem.*, 87:2121–2127, 1983.

[58] T. S. Zwier, E. Carrasquillo, and D. H. Levy. The spectroscopy and single vibronic level fluorescence quantum yields of jet cooled trans-stilbene and its van der Waals complexes. *J. Chem. Phys.*, 78:5493, 1983.

[59] H.-G. Löhmannsröbben, D. Bahatt, and U. Even. Molecular van der Waals complexes with Perylene and Tetracene in the molecular beam. *J. Phys. Chem.*, 94:6286–6290, 1990.

[60] H. T. Jonkman, U. Even, and J. Kommandeur. Organic molecules in a supersonic jet expansion. *J. Phys. Chem.*, 89:4240–4243, 1985.

[61] M. Hillenkamp, S. Keinan, and U. Even. Condensation limited cooling in supersonic expansions. *J. Chem. Phys.*, 118:8699, 2003.

[62] N. Pörtner, A. Vilesov, and M. Havenith. The formation of heterogeneous van der Waals complexes in helium droplets. *Chem. Phys. Lett.*, 343:281–288, 2001.

[63] A. D. Buckingham, P. W. Fowler, and J. M. Hutson. Theoretical studies of van der Waals molecules and intermolecular forces. *Chem. Rev.*, 88:963–988, 1988.

[64] R. E. Smalley, L. Wharton, and D. Levy. Molecular optical spectroscopy with supersonic beams and jets. *Acc. Chem. Res.*, 10:139–145, 1977.

[65] A. Roth. *Vacuum Technology*. North Holland, 1990.

[66] F. Reif. *Fundamentals of statistical and thermal physics*. McGraw Hill, 1965.

[67] C. Kittel. *Introduction to Solid State Physics*. Wiley, 2004.

[68] D. Patterson. *Buffer gas cooled beams and cold molecular collisions*. PhD thesis, Harvard University, 2010.

[69] E. Clementi and G. Corongiu. Van der Waals interaction energies of helium, neon and argon with Naphthalene. *J. Phys. Chem.*, 105:10379–10383, 2001.

[70] M. Hartmann, A. Lindinger, J. P. Toennies, and A. F. Vilesov. The phonon wings in the ($S_1 \leftarrow S_0$) spectra of tetracene, pentacene, porphin and pthalocyanine in liquid helium droplets. *Phys. Chem. Chem. Phys.*, 4:4839–4844, 2002.

[71] Comsol Multiphysics. COMSOL Inc. Burlington, MA 01803.

[72] N. N. Brahms, T. V. Tscherbul, P. Zhang, J. Klos, H.R. Sadeghpour, A. Dalgarno, J. M. Doyle, and T.G. Walker. Formation of van der Waals molecules in buffer gas cooled magnetic traps. *Phys. Rev. Lett.*, 105:033001, 2010.

[73] Y. S. Au, C. B. Connolly, W. Ketterle, and J. M. Doyle. Vibrational quenching of the electronic ground state in ThO in cold collisions with ^{3}He. *arXiv:1310.7279 [physics.atom-ph]*, 2013.

[74] M. M. Beaky, T. M. Goyette, and F. C. De Lucia. Ppressure broadening and line shift measurements of carbon monoxide in collision with helium from 1 to 600 K. *J. Chem. Phys.*, 105:3994–4004, 1996.

[75] Du Jing and Zeng Pan. Molecular vibrational modes of C60 and C70 via finite element method. *Euro. J. Mech. - A/Solids*, 28(5):948–954, 2009.

[76] T. Suzuki, N. Mikami, and M. Ito. Two-color stimulated emission spectroscopy of trans-Stilbene: large amplitude torsional motion in the ground state and its role in intramolecular vibrational redistribution. *J. Phys. Chem.*, 90:6431–6440, 1986.

[77] L. H. Spangler, R. van Zee, and T. S. Zwier. Assignment of the low-frequency modes in trans-Stilbene: evidence for planarity in the isolated molecule. *J. Phys. Chem.*, 91:2782–2786, 1987.

[78] J. A. Syage, W. M. Lambert, P. M. Felker, and A. H. Zewail. Picosecond excitation and trans–cis isomerization of Stilbene in a supersonic jet: Dynamics and spectra. *Chem. Phys. Lett.*, 88:266–270, 1982.

[79] A. Stefanov, A. Stibor, A. Dominguez-Clarimon, and M. Arndt. Sublimation enthalpy of dye molecules measured using fluorescence. *J. Chem. Phys.*, 121:6935–6940, 2004.

[80] P. Greenspan, E. P. Mayer, and S. D. Fowler. Nile Red: a selective fluorescent stain for intracellular lipid droplets. *J. Cell Bio.*, 100:965–973, 1985.

[81] A. Jee, S. Park, H. Kwon, and M. Lee. Excited state dynamics of Nile Red in polymers. *Chem. Phys. Lett.*, 477:112–115, 2009.

[82] C. M. Golini, B. W. Williams, and J. B. Foresman. Further solvatochromic, thermochromic, and theoretical studies on Nile Red. *J. Fluoresc.*, 8:395–404, 1998.

[83] N. A. Murugan and Z. Rinkevicius. Modeling solvatochromism of Nile Red in water. *Int. J. Quantum Chem.*, 111:1521–1530, 2010.

[84] Discussion with Melanie Schnell and Alvin Shubert.

[85] J. Piskorksi, D. Patterson, S. Eibenberger, and J. M. Doyle. Measurement of vibrational relaxation cross sections and observation of dimers in a buffer gas cell. *In prep.*, 2014.

[86] T. Kobayashi, K. Honma, O. Kajimoto, and S. Tsuchiya. Benzonitrile and its van der Waals complexes studied in a free jet. I. The LIF spectra and the structure. *J. Chem. Phys.*, 86:1111, 1987.

[87] H. Saigusa and E. C. Lim. Excitonic interactions and excimer formation in pure and mixed cluster isotopomers of naphthalene. *J. Chem. Phys.*, 103:8793, 1995.

[88] A. D. Buckingham, P. W. Fowler, and J. M. Hutson. Theoretical studies of van der Waals molecules and intermolecular forces. *Chem. Rev.*, 88:963–988, 1988.

[89] G. Quéméner, Balakrishnan N., and A. Dalgarno. Inelastic collsions and chemical reactions of molecules at low temperatures. In *Cold Molecules: Theory, Experiment, Applications*. CRC Press, 2009.

[90] G. M. McClelland, K. L. Saenger, J. J. Valentini, and D. R. Herschbach. Vibrational and rotational relaxation of Iodine in seeded supersonic beams. *J. Phys. Chem.*, 83:947 – 59, 1979.

[91] P. Thistlethwaite. The vibrational analysis of the 274-nm system of Benzonitrile: A reinterpretation. *Aust. J. Chem.*, 30:1595, 1977.

[92] S. Carniato, V. Ilakovac, J.-J. Gallet, E. Kukk, and Y. Luo. Hybrid density-functional theory calculations of near-edge x-ray absorption fine-structure spectra: Applications on Benzonitrile in gas phase. *Phys. Rev. A*, 71:022511, 2005.

[93] M. Schäfer and A. Bauder. Vibrationally excited states in a pulsed jet observed by fourier transform microwave spectroscopy. *Chem. Phys. Lett.*, 308:355–362, 1999.

[94] T. Kobayashi and O. Kajimoto. Benzonitrile and its van der Waals complexes studied in a free jet. III. Enhancement of the intersystem crossing rate in the benzonitrile dimer and other complexes. *Res. Chem. Intermed.*, 24:785–802, 1998.

[95] M. Schmitt, M. Böhm, C. Ratzer, S. Siegert, M. Bo, M. van Beek, and W. L. Meerts. Electronic excitation in the benzonitrile dimer : The intermolecular structure in the S_0 and S_1 state determined by rotationally resolved electronic spectroscopy. *J. Mol. Struct.*, 195:234–241, 2006.

[96] D. R. Borst, T. M. Korter, and D. W. Pratt. On the additivity of bond dipole moments . stark effect studies of the rotationally resolved electronic spectra of aniline , benzonitrile , and aminobenzonitrile. *Chem. Phys. Lett.*, 350:485–490, 2001.

[97] J. Piskorski, D. Patterson, and J. M. Doyle. Cooling, spectroscopy and non-sticking of trans-Stilbene and Nile Red. *In prep.*, 2014.

[98] W.-Y. Chiang and J. Laane. Fluorescence spectra and torsional potential functions for trans-stilbene in its S_0 and $S_1(\pi,\pi^*)$ electronic states. *J. Chem. Phys.*, 100:8755, 1994.

[99] M. Chowdhury and T. Chakraborty. Supersonic jet spectroscopy of floppy molecules. *Proceedings of the Indian Academy of Sciences - Chemical Sciences*, 104:629–633, 2010.

[100] U. Even, J. Magen, J. Jortner, J. Friedman, and H. Levanon. Isolated ultracold porphyrins in supersonic expansions. I. Freebase tetraphenylporphyrin and Zntetraphenylporphyrin. *J. Chem. Phys.*, 77:4374, 1982.

[101] D. W. Werst, W. R. Gentry, and P. F. Barbara. The S_0 and S_1 torsional potentials of 9-Phenylanthracene. *J. Phys. Chem.*, 89:729–732, 1985.

[102] D. Pentlehner, R. Riechers, A. Vdovin, G. M. Pötzl, and A. Slenczka. Electronic spectroscopy of molecules in superfluid helium nanodroplets: an excellent sensor for intramolecular charge redistribution. *J. Phys. Chem. A*, 115:7034–43, 2011.

[103] A. Stromeck-Faderl, D. Pentlehner, U. Kensy, and B. Dick. High-resolution electronic spectroscopy of the BODIPY chromophore in supersonic beam and superfluid helium droplets. *Chem. Phys. Chem.*, 12:1969–80, 2011.

[104] Cryomech PT415 Cryocooler.

[105] E. J. Judge, J. J. Brady, and R. J. Levis. Mass analysis of biological macromolecules at atmospheric pressure using nonresonant femtosecond laser vaporization and electrospray ionization. *Annal. Chem.*, 82:10203–7, 2010.

[106] L. A. Phillips, S. P. Webb, Martinez III, S. J., G. R. Fleming, and D. H. Levy. Time-resolved spectroscopy of tryptophan conformers in a supersonic jet. *J. Am. Chem. Soc.*, 110:1352–1355, 1988.